Two New Concepts to Measure Fluorescence Resonance Energy Transfer via Fluorescence Correlation Spectroscopy: Theory and Experimental Realizations

Jerker Widengren,*,† Enno Schweinberger, Sylvia Berger, and Claus A. M. Seidel*

Department of Spectroscopy and Photochemical Kinetics, Max-Planck Institute for Biophysical Chemistry, Am Fassberg 11, 37077 Göttingen, Germany

Received: January 26, 2001; In Final Form: April 25, 2001

In this study, we demonstrate two new concepts, using fluorescence correlation spectroscopy (FCS), to characterize fluorescence resonance energy transfer (FRET). The two approaches were tested experimentally by measuring a series of double-stranded DNA molecules, with different numbers of base-pairs separating the donor (Alexa488) and acceptor (Cy5) fluorophores. In the first approach, FRET efficiencies are determined from the detected acceptor fluorescence rate per molecule. Here, the unique possibility with FCS to determine the mean number of molecules within the detection volume is exploited, making a concentration calibration superfluous. The second approach takes advantage of FRET-dependent fluorescence fluctuations of photophysical origin, in particular fluctuations generated by trans−cis isomerization of the acceptor dye. The rate of interchange between the trans and cis states is proportional to the excitation rate and can be conveniently measured by FCS. Under FRET-mediated excitation, this rate can be used as a direct measure of the FRET efficiency. The measured isomerization rate depends only on the fluctuations in the acceptor fluorescence, and is not affected by donor fluorescence cross-talk, background, dye labeling efficiencies, or by the concentration of molecules under study. The measured FRET efficiencies are well in agreement with a structural model of DNA. Furthermore, additional structural information is obtained from simulations of the measured fraction of acceptor dyes being in a nonfluorescent cis conformation, from which differences in the position and orientation of the trans and cis form of the acceptor dye can be predicted.

1. Introduction

To be able to understand the functions and the underlying mechanisms of many macromolecules, structural and dynamic information on the molecules in question is needed. Förster fluorescence resonance energy transfer (FRET) is a photophysical process, which can provide a sensitive tool to yield distance information in the range of 10−100 Å. Via FRET, energy is transferred nonradiatively from a donor molecule to an acceptor molecule via induced dipole−induced dipole interaction.

The sensitivity of FRET relies on the fact that the efficiency E with which transfer of excitation energy takes place, depends on the inverse-sixth-power of the distance R_{DA} between the donor and acceptor dye molecules.

After its first observation,[1] the development of the theory,[2] and its introduction as a tool to measure biological distances,[3] FRET has found a wide range of applications in the biomedical field (see refs 4−7 for reviews). By use of microscopic techniques it has been possible to apply FRET to many different microenvironments, with little or no interference of the system under study.[8] In the 1990s strong advances have been made in the field of single molecule detection (SMD) by fluorescence (see refs 9−11 for reviews). By analysis of single molecules, it is possible to find heterogeneities that are difficult to reveal by ensemble measurements. This exquisite sensitivity of fluorescence has also been exploited to detect and analyze FRET on single molecules.[12−19]

Fluorescence correlation spectroscopy (FCS) is a technique, where fluctuations in the detected fluorescence originating from small molecule ensembles are used to obtain information about dynamic processes on the molecular scale.[20−23] After its introduction in the early 1970s, the method for a long time suffered from low signal-to-background levels. However, by the introduction of a confocal detection regime with an enhanced spatial and spectral discrimination,[24−26] the range of applications and the capacity of the FCS technique have strongly increased. In general, FCS can provide dynamic information about a wide range of different molecular processes as long as they manifest themselves as changes in the fluorescence intensity (see refs 27−30 for reviews).

To such processes, belong a broad range of photochemically or photophysically induced nonfluorescent transient states and processes in the time ranges from nanoseconds to milliseconds. These states and processes include photon anti-bunching,[31] electron transfer,[32] triplet states,[33,34] photoinduced transient states in green fluorescent proteins,[35,36] trans−cis isomerization,[37] as well as photodegradation.[38,39]

In 1984, Haas and Steinberg[40] proposed in a theoretical work the use of FCS to monitor intramolecular dynamics by changes in FRET efficiencies. For molecules labeled with a donor and an acceptor fluorophore, a reduced donor fluorescence would be accompanied by an increased acceptor fluorescence intensity in the presence of FRET. Thus, for intramolecular movements that result in variations of the FRET efficiency an anticorrelation would occur between the donor and acceptor fluorescence intensities, where the relaxation time of the anticorrelation reflects the time scale of the intramolecular motion, and its

† Present address: Dept. Med. Biophysics, MBB, Von Eulers väg 8, Karolinska Institutet, 171 77 Stockholm, Sweden. Fax: +49−551−201 1006. Phone: +49−551−201 1087/1774. E-mail: jerker.widengren@mbb.ki.se. E-mail: cseidel@gwdg.de.

10.1021/jp010301a CCC: $20.00
Published on Web 06/23/2001

amplitude scales with the difference in donor−acceptor distances between the intramolecular states. However, only very few reports exist, where this approach has been used experimentally. Correlation analysis of the detected donor and acceptor fluorescence from single molecules have been performed, either according to Haas and Steinberg, as a crosscorrelation between the detected donor and acceptor fluorescence, or as an autocorrelation of the ratio of the detected donor and acceptor fluorescence.[13,41] However, the fluctuations observed could not with certainty be ascribed to variations in the distance between the donor and acceptor dyes, and therefore had to be interpreted with great care.

In this work, we introduce two different FCS-based strategies to measure FRET efficiencies, where no fluctuations of the donor−acceptor distance are required. First, we show the possibility to take advantage of FRET-dependent fluorescence fluctuations of photophysical origin. Particularly useful are fluctuations generated by trans−cis isomerization of the acceptor dye. For the frequently used acceptor dye Cy5, FCS measurements have shown that at direct CW excitation fluorescence fluctuations due to trans−cis isomerization are very prominent, and irrespective of the excitation intensity, 50% of the Cy5 dye molecules are in an essentially nonfluorescent cis state.[37] The rate of interchange between the trans and cis states was found to be proportional to the excitation rate. This indicates that the transitions between the trans and cis states of Cy5 are dominated by photoinduced isomerization and back-isomerization, and a photostationary equilibrium is established between the isomeric forms already at very modest excitation intensities. It also means that the rate of interchange, monitored via FCS, can be used as a measure of the excitation rate. Likewise, under indirect FRET mediated excitation the rate of interchange between the isomers will reflect the excitation rates, and can therefore also be used as a measure for the efficiency with which excitation energy is transferred via FRET from the donor to the acceptor dye molecule.

As an alternative approach, we also show the possibility with FCS to determine FRET efficiencies from the detected acceptor fluorescence rates per molecule. Here, the specific ability of FCS to determine the mean absolute number of fluorophores under investigation is exploited.

Following the description of the experimental setup, we present a theory, where the two approaches to measure FRET efficiencies via FCS are introduced. As a model system, we then applied FCS to a series of double-stranded DNA molecules, where the number of base-pair separating the donor (Alexa 488) and acceptor (Cy5) fluorophores was varied from 4 to 22.

From this study, we conclude that FCS, and in particular the trans−cis isomerization kinetics monitored via FCS, provide a simple and sensitive way by which FRET efficiencies over a broad range can be estimated. The readout parameter, the rate of interchange between the isomeric forms of the Cy5 acceptor dye, depends only on the fluctuations in the acceptor fluorescence and is not affected by donor fluorescence cross-talk, background fluorescence, or the concentration of molecules under study.

2. Method and Materials

The confocal microscopy arrangement used in this study has similar basic features to those previously presented for fluorescence correlation spectroscopy, and other applications of ultrasensitive fluorescence spectroscopy.[24,26,42]

The oligonucleotide samples are excited by an argon-ion laser emitting at 496 nm (Sabre, Coherent, Palo Alto, CA). Alternatively, direct excitation of the acceptor molecules is performed by a krypton-ion laser, operated at 647 nm wavelength (Sabre, Coherent, Palo Alto, CA). After reflection by a dual-band dichroic mirror (502/636DCLP, AHF Analysentechnik) the laser beam is focused by a microscope objective (Olympus 60×, NA 1.2, water immersion). The fluorescence is collected and then refocused by the same objective to the image plane, where a pinhole (radius 35 or 60 μm) is placed. The detection volume is defined by the dimensions of the focused laser beam (0.6 or 1.4 μm in beam waist radius) and the collection efficiency function of the confocal microscope. The collected light is split by a dichroic mirror (620DCLX, AHF Analysentechnik) into the fractions originating from the acceptor (Cy5) and donor (Alexa488) fluorophores. Subsequently, band-pass filters are used (HQ730/140, AHF Analysentechnik, + OG590 long-pass filter (Schott) for Cy5, and HQ535/50, AHF Analyzentechnik, for Alexa488) to discriminate the two fractions of the collected fluorescence from laser light scattered at the excitation wavelength and from Raman scattered light of the solvent molecules. Each of the fractions of the fluorescence light is then detected by two avalanche photodiodes (SPCM AQ-141, EG&G Vandreuil, Quebec, Canada), the output pulses of which are processed online by a PC-based correlator board with time resolution of 12.5 ns (ALV5000 with fast option, ALV GmbH, Langen, Germany).

As a model-system in this study, double stranded DNA was used because of its defined and well-known structure. Alexa488 (donor; Molecular Probes) and Cy5 (acceptor, Amersham-Pharmacia) were used as the FRET pair, offering a large Förster radius and well-separated emission wavelengths between the dyes. Because of their negative charge, interactions between the DNA and the dye molecules are minimized. The DNA-strands were synthesized by the standard aminophosphoramidite technology. In the (+)-strands, Cy5 was attached at a fixed site at the 5′-end via a C_6-linker and a 5′-aminomodifier (C_6). Unlabeled complementary DNA (−)-strands were produced, as well as (−)-strands with different positions of Alexa488, where the dye was attached, also via C_6-linkers, to different thymidine residues (Amino-Modifier C6 dT from Glenresearch). For shorter distances (defined as the number of base-pairs Δ_{bp} separating the labeling sites of the donor and acceptor dyes, where $\Delta_{bp} = 0$ bp for the case that the two dyes are labeled to the same base-pair on opposite strands) a 18 mer with the sequence 5′-d(TGT AAA ACG ACG GCC AGT) (Δ_{bp} = 3,4,5,6,9,15, and 17 bp) or a 27 mer, with the sequence 5′-d(TGT AAA ACG AGA GAG CCT AAA ACG ATC), (Δ_{bp} = 11,13, and 20 bp) was employed. For longer distances (Δ_{bp} = 18,22, and 36 bp) a 37 mer (5′-d(TGT AAA ACG ACG GCC AGT ATC TAG TTA TGA CGA GTA AAT C)) was used. The oligonucleotides were double HPLC-purified and in most cases additionally PAGE-purified. All synthesis (except the Alexa488 postlabeling) and purification were done by IBA GmbH NAPS (Göttingen, Germany). Hybridization was performed in a buffer containing 180 mM NaCl, 12 mM Na-citrate, and 25 μM $MgCl_2$ (pH 7.5). To obtain the FRET-active molecules, complementary donor and acceptor strands were mixed in an 1:1 ratio and slowly cooled from 95 to 20 °C. Donor-only (acceptor-only) molecules were made by hybridizing the Alexa488 (Cy5) labeled strands to a 5-fold excess of the appropriate unlabeled complementary strand. In all FCS experiments, we used a sodium phosphate buffer with 180 mM NaCl, 10 mM NaH_2PO_4/Na_2HPO_4, and 400 μM Na-ascorbate (pH 7.5).

3. Theory

3.1. Fluorescence Correlation Spectroscopy. Generally in fluorescence microscopy, the detected fluorescence is given from

$$F(t) = \int \mathrm{CEF}(\bar{r}) c(\bar{r},t) g k_{10} \Phi_{F1} {}^{1}_{1}\mathrm{N}(\bar{r},t)\, \mathrm{dV} \qquad (1)$$

Here, CEF($\bar{r}$) is the collection efficiency function of the confocal microscope setup, which is determined by the dimensions of the pinhole and the optical properties of the objective, $c(\bar{r},t)$ denotes the concentration of fluorophores, and g accounts for the quantum efficiency of the detectors and the attenuation of the fluorescence in the passage from the sample volume to the detector areas. k_{10} is the deexcitation rate constant from the excited singlet fluorescent state, Φ_F denotes the quantum yield of fluorescence, and ${}^{1}_{1}\mathrm{N}(\bar{r},t)$ is the fraction of the fluorophores in the sample volume element that are in their excited singlet fluorescent states. The product of the three latter parameters corresponds to the fluorescence rate per molecule.

In FCS, the fluctuating fluorescence arising from small quantities of fluorescent molecules is used to obtain information about dynamic processes on the molecular level.[20−23] These fluctuations are analyzed in the form of a normalized autocorrelation (AC) function:

$$G(\tau) = \frac{\langle F(t)F(t+\tau)\rangle}{\langle F\rangle^2} = \frac{\langle [\langle F\rangle + \delta F(t)][\langle F\rangle + \delta F(\mathrm{t}+\tau)]\rangle}{\langle F\rangle^2} = 1 + \frac{\langle \delta F(t)\delta F(\mathrm{t}+\tau)\rangle}{\langle F\rangle^2} \qquad (2)$$

where τ is the correlation time. $F(t)$ signifies the detected fluorescence intensity, where $\delta F(t)$ is the variable, fluctuating part and $\langle F\rangle$ denotes the mean.

The fluorescence fluctuations are caused by changes in the excited singlet fluorescent state population and concentration changes due to translational motion of the fluorophores into and out of the sample volume element. For a wide range of photophysical processes, the generated transient states can be considered nonfluorescent. The normalized AC function for one fluorescent species whose detected fluorescence is given from eq 1 can then be expressed as

$$G(\tau) = 1 + \frac{1}{N_\mathrm{m}}\left(\frac{1}{1+4D\tau/{\omega_1}^2}\right)\left(\frac{1}{1+4D\tau/{\omega_2}^2}\right)^{1/2}\frac{{}^{1}_{1}\mathrm{N}(\tau)}{{}^{1}_{1}\bar{\mathrm{N}}} \qquad (3)$$

The first two factors arise from fluorescence fluctuations generated from translational diffusion of the fluorescent molecules into and out of the detection volume,[24,26,43] where ω_1 and ω_2 are the distances from the center of the laser beam focus in the radial and axial direction respectively at which the collected fluorescence intensity has dropped by a factor of e^2 compared to its peak value. N_m is the mean number of fluorescent molecules within the effective volume of observation $\pi^{3/2}{\omega_1}^2\omega_2$ (the sample volume element), and D is the translational diffusion coefficient of the fluorescent molecules. $\tau_\mathrm{D} = {\omega_1}^2/4D$ approximates the translational diffusion time of the molecules through the sample volume element. Equation 3 assumes the collected fluorescence profile to be Gaussian shaped in the axial as well as in the radial direction. However, eq 3 can also provide a good approximation for a diffraction limited distribution of the excitation intensity in the focal region of the laser beam, when a matching confocal pinhole is used.[26] The last factor of eq 3 takes population of transient nonfluorescent states into account, which leads to changes in the excited singlet state population. Such states can be relatively long-lived, and therefore also significantly populated, leading to saturation of the fluorescence signal. Transitions to and from states of this kind generate fluorescence fluctuations, which are superimposed on those caused by concentration changes due to translational motion of the fluorophores into and out of the sample volume element. In eq 3, ${}^{1}_{1}\mathrm{N}(\tau)$ is the probability that a fluorophore is in its excited singlet fluorescent state at time τ after emission of a photon. ${}^{1}_{1}\bar{\mathrm{N}}$ is the mean probability of all the fluorophores within the sample volume element to be in this state. These parameters provide information about several processes leading to formation of dark transient states, such as intersystem crossing to triplet states, photoinduced charge transfer, and trans−cis isomerization.

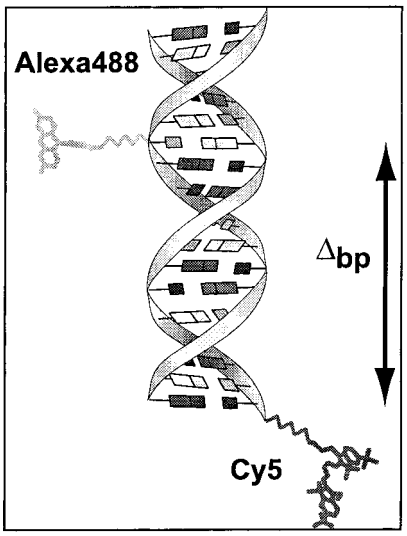

Figure 1. The DNA constructs used in this study. Cy5 (acceptor) was attached to the 5′-end of one of the strands. On the complementary strand, Alexa488 (donor) was attached to different base-pairs with donor−acceptor base-pair separations of Δ_bp = 3, 4, 5, 6, 9, 11, 13, 15, 17, 18, 20, and 22 bp.

3.2. Trans−Cis Isomerization under Direct Excitation Monitored by FCS. The photophysical properties of Cy5 under direct excitation have been treated in detail elsewhere.[37] For Cy5, relaxation processes in the experimental AC curves can be observed due to photoinduced reversible trans−cis isomerization between the fluorescent trans form, denoted N (normal), and a nonfluorescent cis form, denoted P (photoproduct). In addition, fluorescence fluctuations occur, which can be attributed to transitions to and from the lowest triplet state, ${}^{3}_{1}\mathrm{N}$, of the Cy5 molecules. The kinetic schedule of Figure 2a can be used to take these transitions into consideration, and to derive expressions for ${}^{1}_{1}\mathrm{N}(\tau)$ and ${}^{1}_{1}\bar{\mathrm{N}}$ (see eq 3 in ref 37.).

However, based on two assumptions, a considerably simpler model can also be applied. First, if excitation rates are kept low, fluorescence saturation of the Cy5 fluorophores, and the level of triplet state population can be neglected. In addition, since the quantum yields of isomerization following excitation of the trans (N) or cis (P) state are low, the transitions between the ground and excited singlet states of N and P take place on a time scale orders of magnitude faster than that of trans−cis isomerization. The scheme of Figure 2a can then be simplified to that of Figure 2b, containing only two states, the fluorescent trans form N (${}^{1}_{1}\mathrm{N}$ and ${}^{1}_{0}\mathrm{N}$) and the nonfluorescent cis form P (${}^{1}_{1}\mathrm{P}$ and ${}^{1}_{0}\mathrm{P}$). The effective transition rates between the two

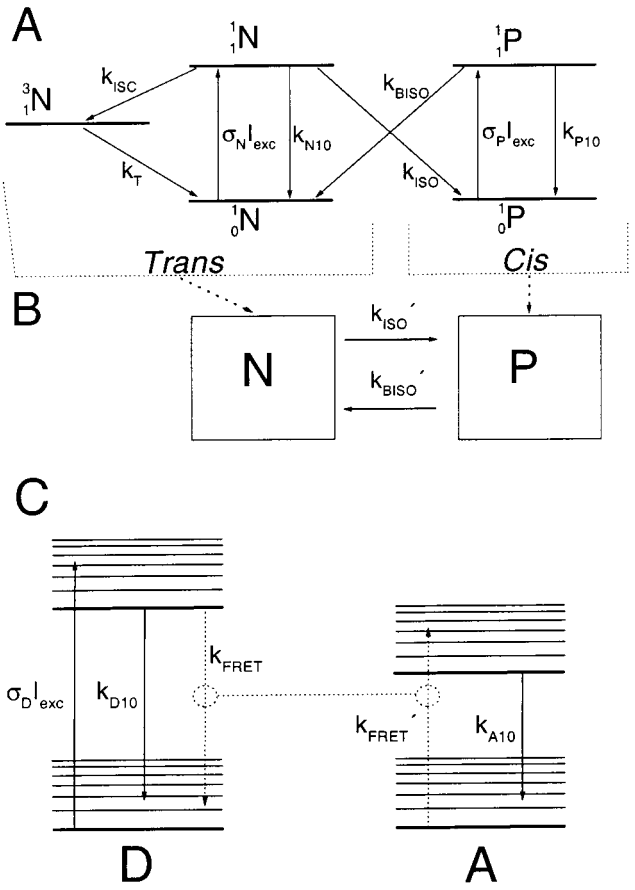

Figure 2. A: Model used to describe the photophysically generated fluorescence fluctuations of Cy5. Here, $^1_0$N, $^1_1$N, and $^3_1$N denote the ground singlet, excited singlet, and the lowest triplet state of the trans isomer. $^1_0$P and $^1_1$P denote the ground and the excited singlet state of the cis isomer. k_{ISC} and k_T are the rate constants for intersystem crossing from $^1_1$N to $^3_1$N, and that of triplet state deactivation back to $^1_0$N. σ_N and σ_P are the excitation cross sections of the trans and the cis isomer. I_{exc} is the excitation intensity experienced by the molecules under study. k_{N10} and k_{P10} are the deactivation rate constants from the excited singlet states ($^1_1$N and $^1_1$P) of the trans and cis conformational states to their ground singlet states ($^1_0$N and $^1_0$P). B: Simplified model applicable under low excitation intensities ($\sigma_N I_{exc} \ll k_{N10}$, $\sigma_N I_{exc} \ll k_{N10}$) containing only two states, the fluorescent trans form N ($^1_1$N and $^1_0$N) and the nonfluorescent cis form P ($^1_1$P and $^1_0$P). k_{ISO}' and k_{BISO}' signify the effective rates of isomerization and back-isomerization between N and P, given by eqs 4 and 5. C: Simplified energy-level diagram for Fluorescence resonance energy transfer (FRET). After excitation of the donor dye D with the excitation rate $\sigma_D I_{exc}$, where σ_D is the excitation cross section of the donor dye and I_{exc} signifies the excitation intensity, deactivation of the excited state of the donor to the ground state takes place via the competing processes k_{D10} (rate constant for fluorescence and internal conversion) or k_{FRET} (rate constant for FRET to the acceptor dye molecule). The acceptor is excited by the effective rate k_{FRET}', given by eq 12.

isomeric forms are then given by

$$k_{ISO}' = \frac{\sigma_N I_{exc}}{\sigma_N I_{exc} + k_{N10}} k_{ISO} = \{\sigma_N I_{exc} \ll k_{N10}\} = \sigma_N I_{exc} \Phi_{ISO} \quad (4)$$

$$k_{BISO}' = \frac{\sigma_P I_{exc}}{\sigma_P I_{exc} + k_{P10}} k_{BISO} = \{\sigma_P I_{exc} \ll k_{P10}\} = \sigma_P I_{exc} \Phi_{BISO} \quad (5)$$

Here, σ_N and σ_P denote the excitation cross sections of the trans and cis forms; I_{exc} is the excitation intensity in the detection volume (assumed to be uniform under our conditions, with a projected pinhole in the object plane smaller than the dimensions of the laser beam, and calculated as the mean intensity within the area of the projected pinhole in the focal plane); k_{N10} and k_{P10} are the deactivation rate constants of the excited state of the trans and the cis form; and k_{ISO} and k_{BISO} are the rate constants of isomerization and back-isomerization from the excited states of the trans and the cis form, respectively. Φ_{ISO} and Φ_{BISO} are the isomerization quantum yields of the trans and cis states, given as the fractions of excitations leading to isomerization and back-isomerization, respectively (i.e., $\Phi_{ISO} = k_{ISO}/(k_{ISO} + k_{N10})$ and $\Phi_{BISO} = k_{BISO}/(k_{BISO} + k_{P10})$). From the effective transition rates of eqs 4 and 5, the fraction of Cy5 molecules within the sample volume element that are in their cis forms $\bar{P}$ and the relaxation rate of the isomerization process k_{ISOtot} are given by

$$\bar{P} = k_{ISO}'/(k_{ISO}' + k_{BISO}') \quad (6)$$

$$k_{ISOtot} = k_{ISO}' + k_{BISO}' = (\sigma_N \Phi_{ISO} + \sigma_P \Phi_{BISO}) I_{exc} \quad (7)$$

From the model of Figure 2b, where the cis form is assumed to be nonfluorescent, and following eq 3, the experimental AC function of the detected fluorescence can be written as

$$G(\tau) = 1 + \frac{1}{N_m}\left(\frac{1}{1 + 4D\tau/\omega_1^2}\right)\left(\frac{1}{1 + 4D\tau/w_2^2}\right)^{1/2} \times \left[1 + \frac{\bar{P}}{1 - \bar{P}} \exp(-k_{ISOtot}\tau)\right] \quad (8)$$

Thus, by fitting the expression of eq 8 to the measured AC curves, $\bar{P}$ and k_{ISOtot} can be obtained, and by use of eqs 6 and 7, k_{ISO}' and k_{BISO}' can be determined.

3.3. Fluorescence Resonance Energy Transfer (FRET). In fluorescence resonance energy transfer (FRET), energy is transferred nonradiatively from a donor molecule to an acceptor molecule via induced dipole−induced dipole interaction. The FRET efficiency E depends on the inverse-sixth-power of the distance R_{DA} between the donor and acceptor dyes:

$$E = k_{FRET}/(k_{FRET} + k_{D10}) = 1/(1 + [R_{DA}/R_0]^6) \quad (9)$$

Here, k_{FRET} is the rate of FRET from the excited state of the donor to the acceptor molecule and k_{D10} denotes the deactivation rate constant of the excited state of the donor fluorophore in the absence of FRET. The constant R_0 is the Förster-radius, defined as the distance at which $E = 50\%$. R_0 depends on the spectroscopic properties of the donor and acceptor dyes and the relative orientation of their transition dipole moments:

$$R_0 = [8.79 \times 10^{-5} J(\lambda) \Phi_{FD} n^{-4} \kappa^2]^{1/6} \text{ [Å]} \quad (10)$$

Here, $J(\lambda)$ is the spectral overlap integral between the fluorescence spectrum of the donor and the excitation spectrum of the acceptor, Φ_{FD} is the fluorescence quantum yield of the donor, and n is the index of refraction of the medium. κ^2 is an orientation factor given by

$$\kappa^2 = [\cos \Theta_T - 3 \cos\Theta_D \cos \Theta_A]^2 \quad (11)$$

where Θ_T is the angle between the unit vectors of the transition moments for the donor $\hat{d}$ and the acceptor $\hat{a}$ and Θ_D denotes the angle between $\hat{d}$ and the separation vector between the

centers of the acceptor and donor transition moments, $R_{DA}\hat{r}$. Θ_A is the corresponding angle between $\hat{a}$ and $R_{DA}\hat{r}$ (see also below, Figure 7C).

3.4. Trans−Cis Isomerization under Indirect, FRET-Mediated Excitation. Under indirect, FRET-mediated excitation of the Cy5 molecules the same unimolecular model as that of Figure 2b can be applied with some modifications of the expressions for the rates of photoinduced isomerization and back-isomerization. Following Figure 2c, the FRET-mediated excitation rate for an acceptor molecule (in its N or P state) is given by

$$k_{FRET}' = \frac{\sigma_D I_{exc}}{\sigma_D I_{exc} + k_{D10} + k_{FRET}} k_{FRET} = \{\sigma_D I_{exc} \ll k_{D10} + k_{FRET}\} = \sigma_D I_{exc} \frac{k_{FRET}}{k_{D10} + k_{FRET}} = \sigma_D I_{exc} E \quad (12)$$

where σ_D is the excitation cross section of the donor fluorophore.

For FRET-mediated excitation, substituting eq 12 into eqs 4 and 5, the transition rates between the two isomeric forms are given by

$$k_{ISO}'(\mathrm{FRET}) = \sigma_D I_{exc} E(\mathrm{N}) \Phi_{ISO} \quad (13)$$

$$k_{BISO}'(\mathrm{FRET}) = \sigma_D I_{exc} E(\mathrm{P}) \Phi_{BISO} \quad (14)$$

Here, E(N) is the FRET efficiency to the trans isomer and E(P) is that to the cis form. As follows from eqs 7, 13, and 14, the measured isomerization relaxation rate k_{ISOtot} can be expressed as a weighted mean of the FRET efficiencies of the trans and the cis isomer, and is proportional to the excitation intensity:

$$k_{ISOtot}(\mathrm{FRET}) = k_{ISO}'(\mathrm{FRET}) + k_{BISO}'(\mathrm{FRET}) = [\sigma_D \Phi_{ISO} E(\mathrm{N}) + \sigma_D \Phi_{BISO} E(\mathrm{P})] I_{exc} \quad (15)$$

3.5. Determination of E from the Measured Trans−Cis Isomerization Rate, k_{ISOtot}. In principle, k_{ISO}'(FRET) and k_{BISO}'(FRET) can be obtained separately from the measured parameters $\bar{P}$ and k_{ISOtot}(FRET) (see eqs 6−8), and E(N) and E(P) can then be determined in absolute terms if σ_D, Φ_{ISO}, and Φ_{BISO} are known. However, from the rates of isomerization and back-isomerization only the products of the excitation cross sections and the isomerization quantum yields are given (eqs 4, 5, 13, and 14). While σ_N is experimentally accessible and also available in the literature, very sparse information about σ_P is found, making it difficult to determine Φ_{BISO}. However, for Cy5 we know from FCS measurements under direct excitation that $\sigma_P \Phi_{BISO} \approx \sigma_N \Phi_{ISO}$ over a broad range of excitation wavelengths.[37] Therefore, we initially assume:

$$\sigma_P = \alpha \sigma_N$$

$$\Phi_{BISO} = \frac{1}{\alpha} \Phi_{ISO} \quad (16)$$

Then, the measured isomerization relaxation rate, as given by eq 15, can be expressed as

$$k_{ISOtot}(\mathrm{FRET}) = \sigma_D I_{exc} \Phi_{ISO} \left[E(\mathrm{N}) + \frac{1}{\alpha} E(\mathrm{P}) \right] \quad (17)$$

Since Φ_{ISO} and Φ_{BISO} have been found to be relatively sensitive to the local environment, in particular the local viscosity, the FRET efficiencies can be experimentally determined by relating the isomerization rates measured under FRET-mediated excitation to those obtained under direct excitation of the acceptor dye in the same molecule, thereby canceling out the contribution of the isomerization quantum yield completely.

From the assumption of eq 16, and by use of eqs 4, 5, and 17, the ratio of k_{ISOtot} measured under indirect FRET-mediated excitation over that measured under direct excitation of the acceptor dye molecules is given by

$$\frac{k_{ISOtot}(\mathrm{FRET})}{k_{ISOtot}} = \frac{\sigma_D(\lambda_D) I_{exc}(\lambda_D) \Phi_{ISO} [E(\mathrm{N}) + 1/\alpha E(\mathrm{P})]}{\sigma_N(\lambda_A) I_{exc}(\lambda_A) \Phi_{ISO} [1 + 1]} \quad (18)$$

where λ_A and λ_D are the excitation wavelengths for direct excitation of the acceptor and indirect FRET-mediated excitation via the donor molecule, respectively. For cyanine dyes similar to Cy5,[44−46] the magnitude of σ_P has been reported to be very similar to that of σ_N. We therefore assume $\alpha = 1$, i.e., $\sigma_P = \sigma_N$. The FRET efficiency can then be calculated from eq 18 as

$$E_{ISO}(\mathrm{N,P}) = \frac{E(\mathrm{N}) + E(\mathrm{P})}{2} = \frac{k_{ISOtot}(\mathrm{FRET})}{I_{exc}(\lambda_D)} \times \left[\frac{k_{ISOtot}}{I_{exc}(\lambda_A)} \right]^{-1} \frac{\sigma_N(\lambda_A)}{\sigma_D(\lambda_D)} \quad (19)$$

This means, with knowledge of the excitation intensities and excitation cross sections, the average FRET efficiency of the two isomeric forms can be obtained as a ratio of the total isomerization rates under FRET-mediated excitation to that under direct excitation. Direct excitation can also be made in the red wavelength range. In this case, the same probe can be used, since no excitation of the acceptor via the donor dye is to be expected. Alternatively, with a reference probe labeled only with an acceptor dye, direct excitation can also be made with the same excitation source as that used for FRET mediated excitation, i.e., $\lambda_A = \lambda_D$.

3.6. The Amplitude of the Isomerization Relaxation Process, $\bar{P}$ in the FCS Curves. Under FRET-mediated excitation, following eqs 13, 14, and 16 the fraction of acceptor molecules being in their cis conformation $\bar{P}$ can be expressed as

$$\bar{P} = \frac{k_{ISO}'(\mathrm{FRET})}{k_{ISO}'(\mathrm{FRET}) + k_{BISO}'(\mathrm{FRET})} = \frac{E(\mathrm{N})}{E(\mathrm{N}) + \frac{1}{\alpha} E(\mathrm{P})} \quad (20)$$

The FRET efficiencies of the trans and the cis states, E(N) and E(P), are given by the resulting Förster radii, R_0(N) and R_0(P), for the FRET from the donor to each of the conformational states. R_0(N) and R_0(P) can be approximated as

$$R_0(\mathrm{N}) = \beta_N(\Delta_{bp}) R_0$$

$$R_0(\mathrm{P}) = \beta_p(\Delta_{bp}) \alpha \delta R_0 \quad (21)$$

Here, R_0 denotes the Förster radius of the trans state if $\kappa^2 = 2/3$. The factors $\beta_N(\Delta_{bp}) = {}^3/_2\kappa^2$ (N,Δ_{bp}) and $\beta_P(\Delta_{bp}) = {}^3/_2\kappa^2$ (P,Δ_{bp}) then take into account the possible variation and deviation from ${}^2/_3$ for the κ^2 orientation factors for the trans and cis isomers (denoted by κ^2(N,Δ_{bp}) and κ^2(P,Δ_{bp}) above), i.e., the possibility that the orientation of the emission and excitation dipole moments of the donor and acceptor dyes are not completely mobile and isotropic, and can depend on the distance in the number of base-pairs Δ_{bp} between the labeling sites of the donor and acceptor dyes. The factor α from eqs 16

and 17 is included in eq 21 to compensate for possible differences in the spectral overlap integral $J(\lambda)$ between the isomeric forms, since $J(\lambda)$ is proportional to the magnitude of the excitation spectrum of the acceptor, and thus to its excitation cross section. The factor δ is introduced to take other differences in $J(\lambda)$ between the trans and cis forms into account, in particular those generated due to a possible spectral shift or shape difference of the excitation spectrum of the cis form compared to that of the trans. From eqs 9, 20 and 21, $\bar{P}$ can then be expressed as

$$\bar{P}(\Delta_{bp}) = \beta_N(\Delta_{bp})R_0^6/[\beta_N(\Delta_{bp})R_0^6 + R_{DA}^6(N,\Delta_{bp})] \times \left[\beta_N(\Delta_{bp})R_0^6/[\beta_N(\Delta_{bp})R_0^6 + R_{DA}^6(N,\Delta_{bp})] + \beta_P(\Delta_{bp})\delta R_0^6/[\beta_P(\Delta_{bp})\alpha\delta R_0^6 + R_{DA}^6(P,\Delta_{bp})]\right]^{-1} \quad (22)$$

Here, $R_{DA}(N,\Delta_{bp})$ and $R_{DA}(P,\Delta_{bp})$ denote the distance between the donor and acceptor dyes when the acceptor is in a trans and in a cis conformation, respectively.

3.7. Determination of *E* from the Measured Acceptor Fluorescence Rate per Molecule. As an alternative approach, the FRET efficiency of a donor−acceptor dye-pair can be estimated from the detected acceptor fluorescence rate per molecule $\bar{F}_{Nm}$. According to eqs 1 and 3:

$$\bar{F}_{Nm} = \frac{\langle F\rangle}{N_m} = \frac{\langle \int \mathrm{CEF}(\bar{r})c(\bar{r},t)gk_{N10}\Phi_{FA1}{}^1\bar{N}(\bar{r})\,dV\rangle}{N_m} \quad (23)$$

where Φ_{FA} is the fluorescence quantum yield of the acceptor dye.

For a uniform excitation intensity, the fraction of molecules in their trans excited singlet state, ${}^1_1\bar{N}(\bar{r})$, is constant and equals ${}^1_1\bar{N}$ within the volume element. $\bar{F}_{Nm}$ can then be written as

$$\bar{F}_{Nm} = \frac{gk_{N10}\Phi_{FA1}{}^1\bar{N}\int \mathrm{CEF}(\bar{r})c(\bar{r},t)\,dV}{N_m} = gk_{N10}\Phi_{FA1}{}^1\bar{N} \quad (24)$$

where the integral $\int \mathrm{CEF}(\bar{r})c(\bar{r},t)\,dV$ equals N_m, and the fraction of dye molecules being in their trans excited singlet states ${}^1_1\bar{N}$ is given by

$${}^1_1\bar{N} = (1-\bar{P}) \times \frac{\sigma_D I_{exc} E(N)}{k_{N10}} \quad (25)$$

Here, the first factor corresponds to the fraction of dye molecules in a trans conformation. The second factor is the fraction of dye molecules in their trans form that are in their excited states, where in analogy to eqs 4, 5, 12−14, low excitation intensities have been assumed. By substitution of eq 25 into eq 24, the fluorescence rate per acceptor dye molecule in the trans state, denoted $\bar{F}_{Nm}(N)$, is given by

$$\bar{F}_{Nm}(N) = \frac{\bar{F}_{Nm}}{(1-\bar{P})} = g\Phi_{FA}\sigma_D I_{exc} E(N) \quad (26)$$

$\bar{F}_{Nm}(N)$ is obtained from the FCS measurements as the detected mean acceptor fluorescence intensity $\langle F\rangle$, multiplied by the total amplitude of the AC curve. This amplitude corresponds to the inverse mean number of molecules in the sample volume element that are in their trans states, $1/(1-\bar{P})N_m$ ($1/N_m$ represents the amplitude of the part of the AC curve which is attributable to fluorescence from translational diffusion only (dotted curves in Figures 3, 4a,b)).

According to eq 26, $E(N)$ can in principle be determined directly from a FCS measurement. However, for an absolute determination of $E(N)$, the overall detection quantum efficiency of the instrumentation g, the fluorescence quantum yield of the acceptor dye Φ_{FA}, and the excitation cross section of the donor σ_D, need to be known.

4. Results and Discussion

In the following section, the two approaches to determine FRET efficiencies from FCS measurements, as given by eqs 19 and 26, were investigated for the series of double stranded DNA molecules described above, where the number of base-pairs separating the donor (Alexa488) and acceptor (Cy5) probes, denoted Δ_{bp}, was varied from 4bp to 22bp. First, the isomerization properties of the oligonucleotide-coupled acceptor dye was investigated under direct excitation at 647 nm and at 496 nm. Thereafter, the rates of isomerization, as well as the detected acceptor fluorescence rates per acceptor dye molecule were investigated under FRET-mediated excitation at 496 nm, where the excitation spectrum of the donor fluorophore is close to its maximum. From these data, FRET efficiencies were calculated. The consistency of the measured and calculated FRET efficiencies were checked against a structural model of the DNA molecules investigated. Finally, the significance and information content of the amplitude $\bar{P}$ of the isomerization relaxation process of the FCS curves were investigated via simulations of $\bar{P}$.

4.1. Isomerization Properties at Direct Excitation of the Acceptor Dyes. In Figure 3, a set of AC curves are shown for an acceptor-only labeled oligonucleotide (18bp long, Cy5 at the 5′-end) excited at 647 nm by a krypton ion laser at different excitation intensities (beam radius 0.8 μm, pinhole radius 35 μm). At excitation intensities below 10kW/cm^2, no significant triplet population build-up is to be expected. The fast time range of the AC curves is then dominated by a relaxation process with a relative total amplitude of the correlation curves of about 50%. This relaxation process can be attributed to photoinduced trans−cis isomerization, and its amplitude corresponds to the fraction of Cy5 fluorophores being in a nonfluorescent cis conformation ($\bar{P}$ of eqs 6 and 8). This fraction remained close to constant over the whole intensity range investigated. The overall relaxation rate is proportional to the applied excitation intensity (insert Figure 3, solid squares). At excitation intensities above 10 kW/cm^2, a second exponential relaxation process can be observed, which increases slightly in amplitude with higher excitation intensities. It originates from triplet state formation of the Cy5 fluorophores. A more detailed investigation of the photodynamic properties of Cy5 has recently been presented.[37] In that study, it was shown that by application of a global fitting routine, where several AC curves measured under different excitation intensities are fitted to expressions of ${}^1_1N(\tau)$ and ${}^1_1N$, based on the model given in Figure 2a, a straightforward way is offered by which the isomerization and triplet state properties of Cy5 can be determined.

In this study, the same global analysis (based on eq 24 of[37]) was applied to the FCS data measured from oligonucleotides containing an acceptor dye only. A series of ten AC curves was measured over an excitation intensity range of 1−100 kW/cm^2 and could be well fitted by the global fitting routine (not shown). From this analysis, the intersystem crossing rate constant to the triplet state, $k_{ISC} = 0.5 \times 10^6 s^{-1}$, and the triplet state deactivation rate constant, $k_T = 0.2 \times 10^6 s^{-1}$, were found to be somewhat lower than those of free Cy5 ($k_{ISC} = 0.8 \times 10^6 s^{-1}$, $k_T = 0.5 \times 10^6 s^{-1}$). This is consistent with a shielding effect of the Cy5

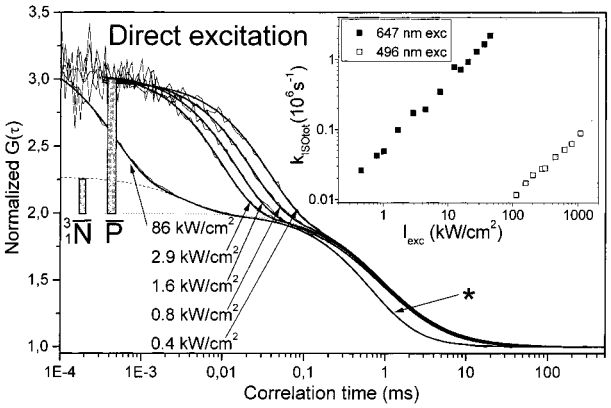

Figure 3. Five AC curves from an 18 bp oligonucleotide with an acceptor dye labeled to the 5′-end of one of the strands, measured under different excitation intensities (0.4, 0.8, 1.6, 2.9, and 86 kW/cm^2) at 647 nm. At excitation intensities below 10 kW/cm^2, the fast time range of the AC curves (<0.1 ms) is dominated by a process attributed to photoinduced trans−cis isomerization. The relative amplitude of this process with respect to the overall amplitude of the correlation curve (right vertical bar) represents the fraction of Cy5 fluorophores being in a nonfluorescent cis conformation ($\bar{P}$ of eq 6). At excitation intensities above 10 kW/cm^2, a second exponential relaxation process can be observed (left vertical bar), which originates from triplet state formation ($^3_1\bar{N}$). Under these conditions, $\bar{P}$ and $^3_1\bar{N}$ can be obtained from the steady-state solution to the kinetic scheme shown in Figure 2a.[37] For the correlation curve measured at 86 kW/cm^2, the apparent diffusion time through the detection volume was shorter, due to photobleaching of the Cy5 dye within the passage time through the detection volume (*). The amplitudes of the AC curves have been normalized so that $N_m = 1$, giving an amplitude of 1 to the part of the AC curves that is generated from translational diffusion only (dotted curve). The dashed curve represents the part of the AC curves being generated from translational diffusion and singlet−triplet transitions. The total amplitude of the AC curve is given by $1/[N_m(1 - \bar{P} - {}^3_1\bar{N})]$, corresponding to the inverse mean number of acceptor dyes in the sample volume element that are in their trans singlet states. Insert: Measured isomerization rates plotted vs irradiance (in kW/cm^2) at direct excitation, showing a linear dependence to the irradiance. The slopes of k_{ISOtot} vs I_{exc} were determined to 0.1 ms^{-1}(kW/cm^2)$^{-1}$ (496 nm excitation, open squares), and to 40 ms^{-1}(kW/cm^2)$^{-1}$ (647 nm excitation, filled squares).

dye by the conjugated oligonucleotide, leading to lower collisional quenching rates by solubilized oxygen molecules. The effective isomerization and back-isomerization cross sections, given by the products of the excitation cross sections, and the isomerization quantum yields of the trans and cis states, $\sigma_N\Phi_{ISO} = 0.063 \times 10^{-16}$cm^2 and $\sigma_P\Phi_{BISO} = 0.066 \times 10^{-16}$cm^2, were found to be about three times lower than those measured for free Cy5. This reflects influence of steric hindrance and an increased viscous drag on the isomerization process when Cy5 is labeled to the oligonucleotide. For the trans conformation, the isomerization quantum yield can be estimated to $\Phi_{ISO} = 7 \times 10^{-3}$, based on an excitation cross section of $\sigma_N = 9.6 \times 10^{-16}$cm^2,[47] which in turn, based on a fluorescence lifetime of 1.4 ns,[48] yields an absolute rate of isomerization from the excited singlet state of the trans form of $k_{ISO} = 5 \times 10^6$s^{-1}. However, for the cis state neither the excitation cross section, nor the excited state lifetime is known in detail. Therefore, only the product of the excitation cross section and the back-isomerization quantum yield can be determined. The obtained parameters are well in agreement with those obtained in ref 37 for the isomerization and triplet state properties of Cy5 conjugated to a similar oligonucleotide.

Under direct excitation at 647 nm, the isomerization properties were also measured for the oligonucleotides labeled with both an acceptor and a donor fluorophore. For base-pair distances between the donor and acceptor dyes of 4−22 bp the relaxation rates and amplitudes of the isomerization process were consistent with those of the acceptor-only labeled molecules. However, a significantly slower (approximately 30%) exchange rate between the trans and cis forms could be observed for the nucleotides having 3 bp distance between the donor and acceptor dyes. The slower rates of isomerization and back-isomerization indicates the presence of steric interactions between the donor and the acceptor dye at this short distance between the dyes.

Direct excitation of acceptor-only oligonucleotides at 496 nm, resulted in a drop of the cis fraction from almost 50% to about 40%, suggesting a relatively higher excitation cross section of the cis form (σ_P) compared to that of the trans form (σ_N) at this excitation wavelength. However, the relatively small variation in the cis fraction observed at different excitation wavelengths indicates that the excitation spectra of the trans and the cis forms to a large extent overlap, which is in line with previous investigations of similar cyanine dyes by other methods.[49] At 496 nm excitation, due to the lower excitation cross sections, σ_N and σ_P, the measured isomerization rates were found to be only 0.3% of those obtained under the same irradiances (in kW/cm^2) at 647 nm (insert, Figure 3). This is well in agreement with the ratio between the excitation rates of Cy5 at 496 and 647 nm excitation found from steady-state fluorescence measurements.

4.2. Isomerization Properties at FRET-Mediated Excitation. The series of double-stranded DNA molecules, as described above, were measured under 496 nm excitation at different excitation intensities, and AC curves of the red acceptor fluorescence were recorded. The excitation intensities were kept low (below 6kW/cm^2) to avoid fluorescence saturation and triplet state formation, both on the donor as well as on the acceptor fluorophores, for all excitation intensities applied and for all the different donor−acceptor base-pair distances investigated. To be able to clearly detect the relaxation process due to trans−cis isomerization within the passage time of the oligonucleotides through the sample volume element ($\tau_D \approx \omega_1^2/4D$), the dimensions of the volume element were also increased by a weaker focusing of the laser beam in the focal plane and by inserting a bigger pinhole in the image plane. In this way, FCS measurements were performed under different excitation intensities with translational diffusion times τ_D of the oligonucleotides of either 0.85−1.25 ms (beam radius 0.6 μm, pinhole radius 35 μm) or 3.0−4.4 ms (beam radius 1.4 μm, pinhole radius 60 μm), where the diffusion times varied for each size of the sample volume element due to different lengths of the oligonucleotide molecules investigated (see method and materials). The dimensions of the projected pinholes in the focal plane were similar or smaller than those of the laser beam in order to validate the assumption of a uniform excitation intensity within the sample volume element.

In Figure 4a, three AC curves are shown for an oligonucleotide with $\Delta_{bp} = 11$ bp, measured at 496 nm excitation with the excitation intensities 1.8, 3.5, and 5.8 kW/cm^2. As for photoinduced trans−cis isomerization at direct excitation of the acceptor dyes, an exponential relaxation process appears whose amplitude is close to constant over the whole excitation intensity range, and whose relaxation rate scales with the applied excitation intensity. We therefore attribute this process to FRET-excitation-induced transitions between the trans and cis forms of the Cy5 acceptor molecules.

In Figure 4b, a set of AC curves are shown which are measured under the same excitation intensity (5.8 kW/cm^2) for oligonucleotides with different donor−acceptor distances (Δ_{bp}

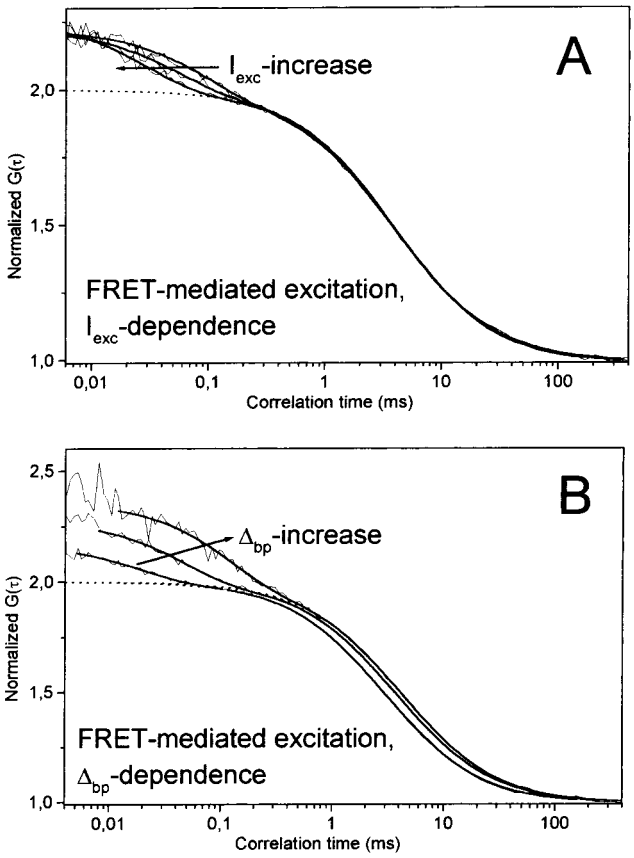

Figure 4. A: Three AC curves, with N_m normalized to 1, measured for an oligonucleotide with $\Delta_{bp} = 11$bp at 496 nm excitation with the excitation intensities 1.8, 3.5, and 5.8 kW/cm^2. In addition to translational diffusion (dotted line), a relaxation process is reflected in the AC curves that can be attributed to FRET-excitation-induced transitions between the trans and cis forms of the Cy5 acceptor molecules. The experimental AC curves shown yielded the following fitting parameters: mean population of cis isomers $\bar{P} = 0.19$, translational diffusion times of the oligonucleotides $\tau_D = \omega_1^2/4D = 3.9$ ms, and isomerization relaxation rates, k_{ISOtot}, of 10.4, 19.2, and 34.8 ms^{-1} for the excitation intensities 1.8, 3.5, and 5.8 kW/cm^2, respectively. B: Three AC curves, with N_m normalized to 1, measured at the same excitation intensity (5.8 kW/cm^2) at 496 nm excitation for oligonucleotides with different donor−acceptor distances (Δ_{bp} of 4, 11, and 18bp). The contribution in the AC curves from translational diffusion is shown as dotted lines. The relaxation rate of the trans−cis isomerization process, k_{ISOtot}, decreases with increasing Δ_{bp} (56.4, 22.0, and 10.0 ms^{-1} for Δ_{bp} of 4, 13, and 18bp, respectively). The relative amplitude of the isomerization relaxation process in the AC curves, also varies with Δ_{bp} (0.15, 0.21 and 0.27, for Δ_{bp} of 4, 13, and 18 bp, respectively). The difference in the diffusion times are due to the different lengths of the oligonucleotides (3.1, 3.8, and 4.1 ms, for the oligonucleotides with lengths 18bp ($\Delta_{bp} = 4$), 27bp ($\Delta_{bp} = 13$), and 37bp ($\Delta_{bp} = 18$), respectively).

of 4, 11, and 18 bp). One can note that the relaxation rate of the trans−cis isomerization process in the fluorescence AC curves decreases with increasing Δ_{bp}, in agreement with an expected decrease of the FRET efficiencies E between the donor and acceptor dyes with larger Δ_{bp}. It can also be noted that the relative amplitudes of the isomerization relaxation process in the AC curves, which reflects the relative population of cis states, are significantly lower than those measured under direct excitation of the acceptor dyes (see Figure 3), and also varies with Δ_{bp}.

For each Δ_{bp}, the measured isomerization relaxation rates k_{ISOtot}(FRET) were plotted vs the applied excitation intensity I_{exc} (Figure 5a). In agreement with eq 15, k_{ISOtot}(FRET), was

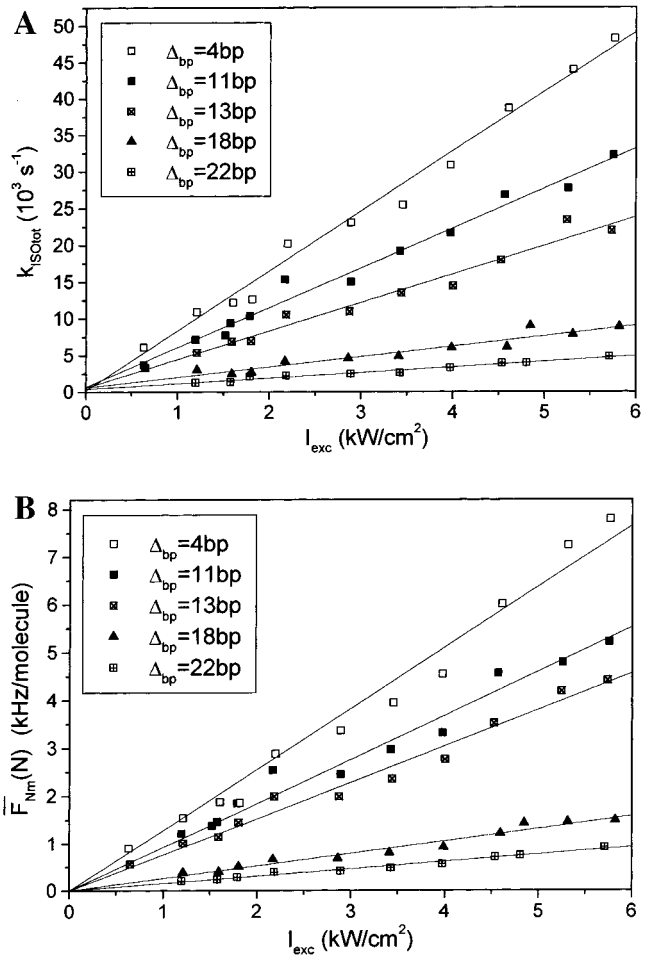

Figure 5. A: The measured isomerization relaxation rates, k_{ISOtot}, plotted vs the applied excitation intensity, I_{exc} for five different oligonucleotides ($\Delta_{bp} = 4$,11,13,18, and 22). For each oligonucleotide measured, k_{ISOtot} shows a distinct linear dependence to I_{exc}. The slopes were determined to: 8.2, 5.4, 3.9, 1.3, and 0.75 ms^{-1}(kW/cm^2)$^{-1}$, for $\Delta_{bp} = 4$, 11, 13, 18, and 22, respectively. B: The detected fluorescence emission rate per acceptor dye molecule in its trans conformation, $\bar{F}_{Nm}$(N), plotted vs excitation intensity for five different oligonucleotides ($\Delta_{bp} = 4$, 11, 13, 18, and 22). For all the oligonucleotides investigated, $\bar{F}_{Nm}$(N) increased linearly to the applied excitation intensity over the range of intensities applied (the excitation intensity below the range of saturation), with slopes ranging from 150 Hz/(kW/cm^2) ($\Delta_{bp} = 22$) to 1.2 kHz/(kW/cm^2) ($\Delta_{bp} = 4$) (see Table 1).

found to show a distinct linear dependence to I_{exc}. The slope of k_{ISOtot}(FRET), vs I_{exc}, dk_{ISOtot}(FRET)/dI_{exc}, should correspond to $\sigma_D\Phi_{ISO}E(N) + \sigma_D\Phi_{BISO}E(P)$ (eq 15) and was found to decrease with longer Δ_{bp}, in agreement with an expected decrease of E(N) and E(P) with longer distances between the donor and acceptor dyes. The calculated slopes dk_{ISOtot}(FRET)/dI_{exc} for all the oligonucleotides are summarized in Table 1.

4.3. Registration of Acceptor Fluorescence Rates per Dye Molecule under FRET-Mediated Excitation. In Figure 5b, the detected fluorescence rate per acceptor dye molecule in the trans state $\bar{F}_{Nm}$(N) is plotted vs excitation intensity for the same set of oligonucleotides as in Figure 5a. Following eq 23−26, $\bar{F}_{Nm}$(N) is obtainable as the mean number of detected fluorescence photons per time unit, $\langle F \rangle$, multiplied by the total amplitude of the measured AC curves. Since the excitation intensities applied were kept low (below 6 kW/cm^2), a significant nonlinear response, such as saturation or triplet state build-up, could be observed neither on the donor nor on the acceptor dyes. In agreement with this, $\bar{F}_{Nm}$(N) increased linearly to the

TABLE 1: Measured and Calculated Parameter Values Obtained under FRET-Mediated Excitation at 496 nm for Different Distances in Base-Pairs Δ_{bp} between the Donor and Acceptor Dyes, or under Direct Excitation at 496 and 647 nm

Δ_{bp}	$dk_{ISOtot}(FRET)/dI_{exc}$ $(ms^{-1}/(kW/cm^2))^a$	$d\bar{F}_{Nm}(\bar{N})/dI_{exc}$ $(kHz/(kW/cm^2))^a$	$\bar{P}$	$E_{ISO}(N,P)$ ($\lambda_A = 647$ nm)	$E_{ISO}(N,P)$ ($\lambda_A = 496$ nm)	$E_{ISO}(N,P)$ scaled[b]	$E_{FNm}(N)$ scaled[c]
4	8.2	1.23	0.147	1.24	1.45	0.92	0.85
5	7.9	1.21	0.156	1.20	1.41	0.89	0.84
6	7.2	1.08	0.161	1.09	1.17	0.79	0.74
9	6.4	1.04	0.178	0.97	1.13	0.71	0.71
11	5.4	0.92	0.191	0.81	0.95	0.60	0.62
13	3.9	0.76	0.220	0.58	0.68	0.43	0.50
15	1.8	0.35	0.248	0.27	0.32	0.20	0.21
17	1.1	0.17	0.263	0.16	0.20	0.12	0.10
18	1.3	0.26	0.258	0.19	0.23	0.14	0.15
20	0.93	0.21	0.238	0.13	0.16	0.10	0.10
22	0.75	0.15	0.225	0.11	0.13	0.08	0.07
36	- - - -	0.06					0.04
direct exc							
496 nm	0.1	0.016	0.38				
647 nm	40	6.5	0.49				

[a] Raw data without subtraction of contributions from direct excitation, donor cross-talk and background. [b] Scaling factor 0.74 (647 nm) and 0.58 (496 nm). [c] Scaling factor 0.69 $(kHz/(kW/cm^2)^{-1}$.

applied excitation intensity over the range of intensities applied, and for all the oligonucleotides investigated. In Table 1, the slopes of $\bar{F}_{Nm}(N)$ vs I_{exc}, $d[\bar{F}_{Nm}(N)]/dI_{exc}$, for all the investigated oligonucleotides are given. According to eq 26, the slopes correspond to $g\Phi_{FA}\sigma_D E(N)$, and decreased with longer Δ_{bp}, reflecting a lower $E(N)$ with increasing donor−acceptor dye distances.

4.4. Calculation of Absolute FRET Efficiencies from the Measured Data. From the plots shown in Figures 5a,b, it can be seen that the measured isomerization relaxation rates k_{ISOtot} as well as the calculated fluorescence count rates per trans acceptor molecule $\bar{F}_{Nm}(N)$ for one oligonucleotide can be well separated from that of another over the whole scale of FRET efficiencies, also for oligonucleotides where the difference in donor−acceptor distances is only two base-pairs.

4.4.1. Calculation of $E_{ISO}(N,P)$. As given by eqs 15 and 17, the slope $dk_{ISOtot}(FRET)/dI_{exc}$ is proportional to a weighted mean of $E(N)$ and $E(P)$. Although cross-talk due to additional donor fluorescence and background scatter can be expected to contribute to the total amount of light registered in the detectors for the acceptor dye fluorescence, these light sources do not produce the fluctuations specific for trans−cis isomerization. In other words, the rates of isomerization and back-isomerization within the acceptor dye are proportional to the excitation rates, but isomerization and back-isomerization take place independent of the level of cross-talk and background, which therefore need not be taken into consideration. In this study, direct excitation at 496 nm of the acceptor-only labeled oligonucleotides gave a contribution to the isomerization rates corresponding to a FRET efficiency of 1% (Table 1).

After subtraction of this contribution from $dk_{ISOtot}(FRET)/dI_{exc}$, and assuming the factor α in eq 17 to equal 1, an absolute FRET efficiency $E_{ISO}(N,P)$ can be calculated from the isomerization rates according to eq 19. The slopes of $k_{ISOtot}(FRET)$ vs I_{exc}, derived above (Figure 5a), corresponds to the first factor of eq 19. As the second factor of eq 19, the slopes of k_{ISOtot} vs I_{exc} for direct excitation of the acceptor dyes at either 647 or 496 nm excitation can be used (inset, Figure 3). In the third factor of eq 19, the ratio of the excitation cross sections of the acceptor at direct excitation over that of the donor was calculated from the values $\sigma_N(647\text{ nm}) = 9.6 \times 10^{-16}$ cm^2,[47] $\sigma_N(496\text{ nm}) = 0.04 \times 10^{-16}$ cm^2 (from steady-state fluorescence measurements), and $\sigma_D(496\text{ nm}) = 2.7 \times 10^{-16}$ cm^2.[50]

Independent of what excitation wavelength that was used (496 or 647 nm) for the direct excitation reference measurement, the absolute FRET-efficiencies derived via eq 19 were found to clearly exceed unity (see Table 1). A comparison to the FRET efficiencies determined by us for the same set of molecules by spectrally resolved, single-molecule fluorescence lifetime measurements[51] also indicates that the FRET efficiencies determined in this study are overestimated by approximately 40 (647 nm excitation as reference) to 60% (496 nm excitation as reference). To compensate for this overestimation, a common scaling factor was introduced to scale the calculated $E_{ISO}(N, P)$ to the FRET efficiencies obtained in ref 51 (see Table 1). In Figure 6 (solid squares), the resulting calculated and scaled $E_{ISO}(N, P)$ are plotted vs Δ_{bp}. The relative changes of $E_{ISO}(N,P)$ with Δ_{bp} were found to be very well in agreement with the FRET efficiencies determined in ref 51, and could be accurately fitted to a DNA helical model (for details see below). The reason for the systematic overestimation of $E_{ISO}(N, P)$ is at present not quite clear. It can be attributed to uncertainties in the determination

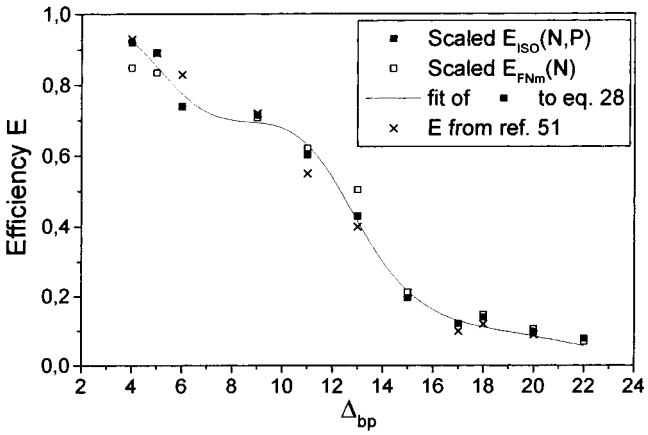

Figure 6. Measured and calculated FRET efficiencies obtained from the isomerization kinetics of the acceptor dyes (solid squares). The FRET efficiencies could be well fitted to a model based on the structure of a double-stranded DNA in aqueous solution (solid lines) by use of eq 28, resolving also the helical structure of the oligonucleotides. The following parameters were generated in the fit: $L = 4$ Å, $z_{bp} = 3.4$ Å (fixed), $d_{rA} = 6$ Å, $d_{rD} = 28$ Å, $\Psi = 308°$, $\phi_1 = 36°$ (fixed), $R_0 = 51$ Å (fixed, obtained from steady-state fluorescence measurements). The relative changes of $E(N)$, calculated via $\bar{F}_{Nm}(N)$ from eq 26, (open squares) were found to be well in agreement with the FRET efficiencies calculated via the isomerization kinetics. For reference, the FRET efficiencies determined via spectrally resolved single molecule fluorescence lifetime measurements for the same molecules [51] have been included (crosses).

TABLE 2: Anisotropies (from Steady-State Fluorescence Measurements) r, Fluorescence Lifetimes (from Time-Correlated-Single-Photon-Counting Measurements) τ_f, and Rotational Correlation Times (calculated via the Perrin equation from r and τ_f with $r_0 = 0.385$) ρ for Alexa488 and Cy5 Conjugated to an Oligonucleotide (18bp), and for Alexa488 and Cy5 Free in Aqueous Solution

	excitation wavelength (nm)	anisotropy, r	fluorescence lifetime τ_f (ns)	rotational correlation time ρ (ns)
Alexa 488	496	0.018	3.8	0.2
DNA-Alexa 488 (18bp)	496	0.05	3.8	0.6
Cy 5	647	0.13	1.0	0.5
DNA- Cy 5 (18bp)	647	0.23	1.4	2.3

of the excitation intensities I_{exc} as well as of the excitation cross section of the acceptor at 496 nm σ_N(496 nm). However, effects due to a scaling factor α less than unity (eq 16), and additional photochemical processes influencing the isomerization kinetics, can also contribute to an overestimation of E. The finding that the fraction of acceptor dyes in a cis conformation $\bar{P}$ is significantly lower under FRET-mediated compared to that found under direct excitation of the acceptor dyes supports the hypothesis that such an additional pathway for back-isomerization exists (see Figure 4b and results and discussion below).

4.4.2. Calculation of E(N) from $\bar{F}_{Nm}(N)$. To estimate the FRET efficiencies from the detected fluorescence rate per acceptor molecule in the trans state $\bar{F}_{Nm}(N)$, the slope $d\bar{F}_{Nm}(N)/dI_{exc}$ (Figure 5b) of an oligonucleotide with $\Delta_{bp} = 36$ was used for corrections. Practically no FRET is expected to be generated within this oligonucleotide. Its slope $d\bar{F}_{Nm}(N)/dI_{exc}$ instead originates from cross-talk of donor fluorescence into the detection channels of the acceptor fluorescence, acceptor fluorescence resulting from direct excitation of the acceptor dyes, and background scatter. In our case, the donor fluorescence cross-talk is the dominating source. Altogether, the slope $d\bar{F}_{Nm}(N)/dI_{exc}$ for this oligonucleotide corresponded to almost 5% of that obtained for the most FRET active oligonucleotides investigated here. This contribution to the slopes is present for all the oligonucleotides, but since the donor fluorescence is quenched by FRET, the donor fluorescence cross-talk will be diminished with increasing E. After correction for this effect, the contributions were subtracted from the slopes of $d\bar{F}_{Nm}(N)/dI_{exc}$ for each oligonucleotide. The slopes were then normalized with a common factor (see Table 2) to fit the FRET efficiencies measured via the isomerization kinetics. From this factor, corresponding to $g\Phi_{FA}\sigma_D$ (eq 26), and with Φ_{FA} set to 0.35[51] and σ_D to 2.7×10^{-16}cm^2,[50] an absolute detection quantum yield, g, of about 1% can be derived, which compares relatively well with the expected g. The relative changes of E calculated from $d\bar{F}_{Nm}(N)/dI_{exc}$ (Table 1 and Figure 6 (open squares)), denoted $E_{FNm}(N)$, are in agreement with the normalized FRET efficiencies calculated via the isomerization kinetics, $E_{ISO}(N, P)$, which reflect a mean of $E(N)$ and $E(P)$ (Table 1 and Figure 6 (solid squares)). The observations for the amplitude $\bar{P}$ of the isomerization process in the AC curves (see below) indicate that $E(N)$ and $E(P)$ are not identical, which should also be reflected in a difference between $E_{ISO}(N,P)$ and $E_{FNm}(N)$. However, although $E_{ISO}(N,P)$ and $E_{FNm}(N)$ in Figure 6 are not fully identical, a systematic difference between $E_{ISO}(N,P)$ and $E_{FNm}(N)$ can also not with certainty be seen beyond the relative error estimates. For $E_{ISO}(N,P)$ and $E_{FNm}(N)$, we estimate the relative errors from the standard error estimates made in the linear fits of $dk_{ISOtot}(FRET)/dI_{exc}$ and $d\bar{F}_{Nm}(N)/dI_{exc}$ (Figures 5a,b) to be between 3 (low Δ_{bp}) and 10% (high Δ_{bp}).

4.5. Consistency of the Measured Relative FRET Efficiencies to a Structural Model. The FRET efficiencies obtained via trans−cis isomerization kinetics were fitted to a model based on the structure of a double-stranded B-DNA in aqueous solution.[52,53] In this model, given the labeling sites of the donor and acceptor dyes, and with reference to Figure 7A,B, the distance R_{DA} between the dyes can be estimated as

$$R_{DA} = \sqrt{(L + \Delta_{bp}z_{bp})^2 + ({d_{rA}}^2 + {d_{rD}}^2 - 2d_{rA}d_{rD}\cos(\Psi + \Delta_{bp}\phi_{bp}))} \quad (27)$$

Here, L accounts for the fact that the projections of the molecular centers of the donor and acceptor fluorophores onto the DNA helical axis does not necessarily correspond with the planes of the base-pairs to which the fluorophores are attached. L then represents the distance along the helical axis for the hypothetical case that the donor and acceptor fluorophores would be attached to the same base-pair ($\Delta_{bp} = 0$). z_{bp} is the length between two base-pairs along the helical axis (fixed to 3.4 Å), and d_{rD} and d_{rA} signify the normal distances from the donor and the acceptor fluorophores to the helical axis. Taking the cylindrical angle of the donor linker arm as a reference point, Ψ is the cylindrical displacement angle of the linker arm of the acceptor fluorophore for $\Delta_{bp} = 0$, and ϕ_{bp} denotes the cylindrical twist angle of the acceptor linker arm per base-pair separating the donor and acceptor linker arms (set to 36° per base-pair). Introducing eq 27 into eq 9 yields an expression for the FRET efficiency between the donor and acceptor fluorophores as a function of base-pair separation:

$$E = \left[\frac{[(L + \Delta_{bp}z_{bp})^2 + ({d_{rA}}^2 + {d_{rD}}^2 - 2d_{rA}d_{rD}\cos(\Psi + \Delta_{bp}\phi_{bp}))]^3}{{R_0}^6} + 1\right]^{-1} \quad (28)$$

In this model, the orientation of the emission and excitation dipole moments of the donor and acceptor fluorophore, respectively, are assumed to be isotropic. Then the κ^2 orientation factor (eq 10) is constant and equals $^2/_3$ over the whole range of Δ_{bp}.

The FRET efficiencies derived from the isomerization kinetics (eq 19) could, after scaling, be well fitted to the model above and eq 28. The fitted curve is shown in Figure 6. The helical structure of the oligonucleotides can be well resolved as a modulation of the FRET-efficiency vs Δ_{bp}. This indicates that both the donor as well as the acceptor dye are separated radially from the DNA helical axis (i.e., that d_{rA} and $d_{rD} \neq 0$). However, since the expression of eq 28 is symmetric with respect to d_{rA} and d_{rD}, the covariance between their fitted values is very strong and an identical fit would be obtained by exchanging the fitted values of d_{rA} and d_{rD}.

4.6. Measured Amplitude of the Isomerization Process in the AC Curves, $\bar{P}$. Under FRET-mediated excitation, the amplitudes of $\bar{P}$ showed several specific features (Figure 8a). First, the amplitudes were found to be considerably lower than those measured under direct excitation of the acceptor dyes (between 0.15 and 0.27, compared to 0.5 at direct excitation at 647 nm). Moreover, an overall increase of $\bar{P}$ was observed with lower FRET efficiencies (longer donor−acceptor dye distances). Finally, superimposed on this overall increase of $\bar{P}$, a periodic

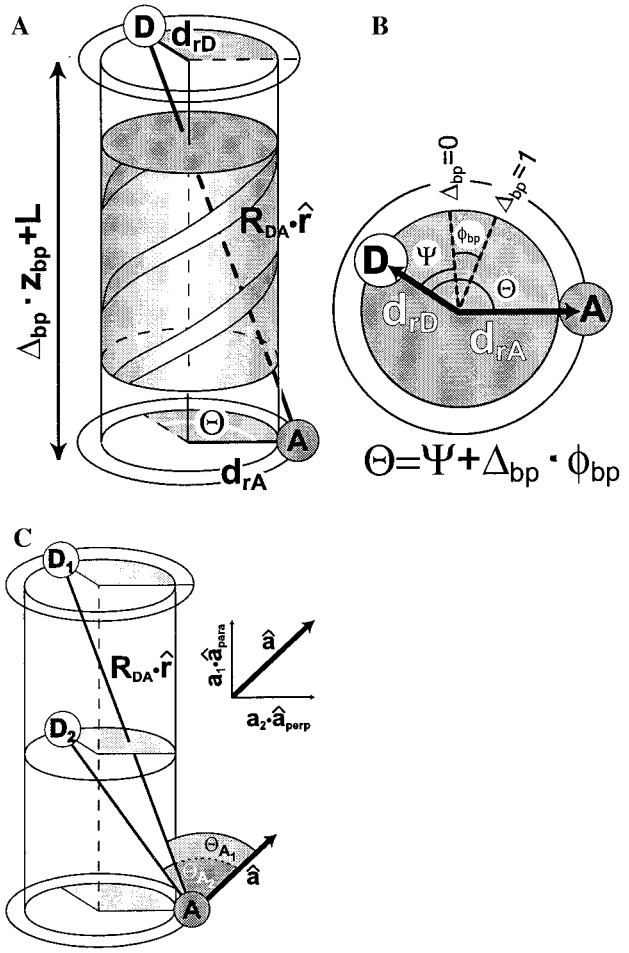

Figure 7. DNA helical model used to calculate the FRET-efficiencies (eqs 27 and 28), as well as to simulate the dependence of $\bar{P}$ on Δ_{bp} (Figures 8 and 9). A: Side-view. B: Cross section of the helix with the helical axis in the center. In the figures, d_{rA} and d_{rD} denote the normal distances from the acceptor A and donor D dyes to the DNA helical axis. $L + \Delta_{bp}z_{bp}$ is the total distance between the donor and acceptor dyes projected along the DNA helical axis, and â represents the unit vector for the direction of the emission dipole moment of A. $R_{DA}\hat{r}$ is the separation vector between the donor and acceptor dyes, where R_{DA} represents the absolute distance between the dyes, and $\hat{r}$ is the unit vector of the separation vector. Θ_A represents the angle between â and $\hat{r}$, and $\Theta = \Psi + \Delta_{bp}\Phi_{bp}$ signifies the angle between the normal separation vectors of the donor and the acceptor. In part C, â has been depicted as it was assumed to be oriented in the simulations of $\bar{P}$ (Figures 8A−E), with two component vectors, one parallel to the helical axis ($a_1\cdot\hat{a}_{para}$), and the other perpendicular to the DNA helical axis and parallel to the normal separation vector for Cy5 ($a_2\cdot\hat{a}_{perp}$). $\hat{d}$ (the unit vector for the excitation dipole moment of the donor dye) was assumed to be isotropic. Depending on Δ_{bp}, Θ_A changes in a nonperiodic manner (illustrated by the difference between the angles Θ_{A1} and Θ_{A2} for the donor positions D_1 and D_2), yielding a nonperiodic change of the κ^2 orientation factor.

variation of $\bar{P}$ over Δ_{bp}, with a period of 10bp, could be noticed. A variation should reflect a relative change of the effective rate constant for isomerization k_{ISO}' vs that for back-isomerization k_{BISO}', which in turn can result from a relative change of E(N) vs E(P) (eq 20). The observed period of 10bp coincides with the number of base-pairs needed to complete a full turn (36° turn per base-pair) in the double stranded oligonucleotide, providing evidence that the amplitude of $\bar{P}$, and its variation with Δ_{bp}, contains structure-related information.

At this point, it is worth to consider that a transition of the acceptor dye from a trans to a cis conformation, and vice versa, represents a considerable structural change within the dye. It would therefore not be surprising if the orientation of the excitation dipole moment of the trans form is different from that of the cis form. Moreover, steric restrictions and electrostatic interactions between the dye, the linker arm and the DNA molecule can be different for the trans and cis forms. Depending on if the dye is in a trans or in a cis conformation, the dye and its linker arm may therefore arrange differently in space. Consequently, for a given labeling site of the acceptor dye, both the distance between the donor and acceptor dyes R_{DA} as well as the κ^2 orientation factor can be different for the trans and the cis forms, leading to an overall shift as well as a periodicity of $\bar{P}$.

4.7. Simulations of $\bar{P}$. To further investigate what principal information is contained in $\bar{P}$, simulations of $\bar{P}$ were performed, where effects of orientation and structure, as well as influence of spectroscopic parameters were considered. $\bar{P}$ was calculated from eq 22, where the distance between the donor and acceptor dyes, $R_{DA}(N,\Delta_{bp})$ and $R_{DA}(P,\Delta_{bp})$, were calculated from eq 27. A scaling factor was added to take the observed overall reduction of $\bar{P}$ into account (see also sections 4.7.6 and 4.7.7).

4.7.1. Model for the κ^2 Orientation Factor: In the simulations, a simplified model for the variation of the κ^2 orientation factors for the trans and the cis states was assumed. For Alexa488 conjugated to the oligonucleotides, a short rotational correlation time ρ was found from steady-state fluorescence measurements (Table 2). This lead us to assume that the orientation of the transition dipole moment of the donor dye $\hat{d}$ is isotropic. For the conjugated Cy5 on the other hand, a considerably longer ρ was found, indicating a more restricted mobility. The orientation of the excitation dipole moment of the acceptor dye â is therefore not assumed to be isotropic. Instead, â is modeled as a linear combination of two vectors, one parallel to the DNA helical axis $\hat{a}_{para}$ and the other perpendicular to this axis and parallel to the normal separation vector between the dye and the DNA helical axis $\hat{a}_{perp}$ (see Figure 7C):

$$\hat{a} = \mathbf{a_1}\hat{a}_{para} + \mathbf{a_2}\hat{a}_{perp} \tag{29}$$

Given that the emission dipole moment of the donor is isotropic, and the excitation dipole moment of the acceptor is fixed in a linear direction, the κ^2 orientation factor can be expressed as[4]

$$\kappa^2 = {}^1/_3 + (\hat{a}\cdot\hat{r})^2 = {}^1/_3 + \cos^2\Theta_A \tag{30}$$

where $\hat{r}$ is the direction of the separation vector between the donor and acceptor dyes, and θ_A is the angle between $\hat{r}$ and â (see eq 11 and Figure 7C). In Appendix 1, an expression for the κ^2 orientation factor is given based on the structural parameters of our DNA model. This expression was used when the Förster radius, R_0, of the trans and cis states were calculated via $\beta_N(\Delta_{bp})$ and $\beta_P(\Delta_{bp})$ of eq 21.

4.7.2. Simulation of $\bar{P}$ with Constrained Parameter Values. In Figure 8A, a simulation of $\bar{P}$ is shown, which is based on the above model for the κ^2 orientation factor, and calculated from eqs 22 and 27. In the simulations, both the resulting vectors for the transition moment of the acceptor dye, given by $\mathbf{a_1}$ and $\mathbf{a_2}$, the length of the normal separation vector of the acceptor from the DNA helical axis d_{rA}, the radial angle between this vector and that of the donor for $\Delta_{bp} = 0$, Ψ, as well as the projection of the linker arm along the DNA helical axis, contained in the parameter L (eq 27), were allowed to be different for the trans and the cis conformation of the acceptor dye. The differences in the latter parameter values between the cis and trans forms are denoted $\Delta d_{rA} = d_{rA}(P) - d_{rA}(N)$, $\Delta\Psi = \Psi(P) - \Psi(N)$ and $\Delta L = L(P) - L(N)$, respectively. To keep

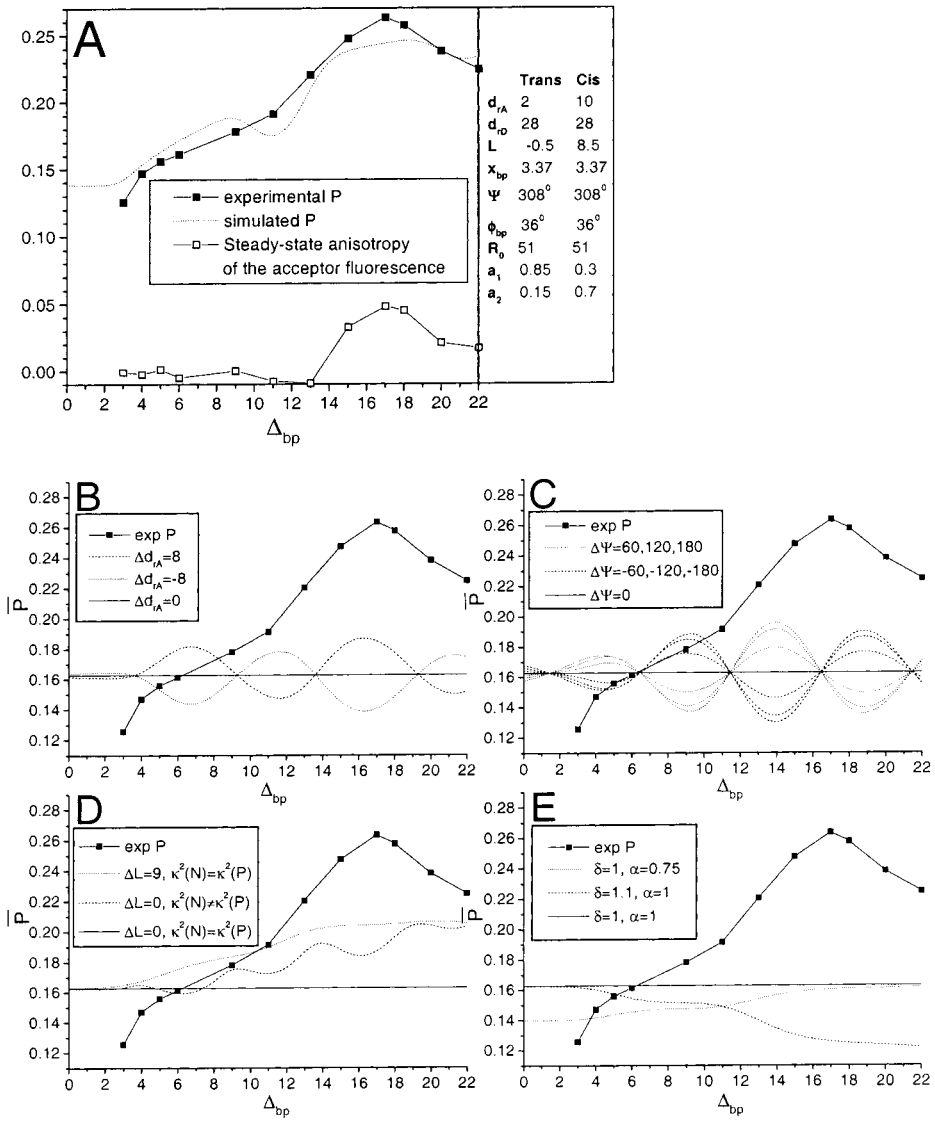

Figure 8. A: Experimental (solid line, solid squares) and simulated (dotted line) curves of $\bar{P}$, as well as the steady-state anisotropy measured for the acceptor fluorescence (solid line, open squares) plotted vs Δ_{bp}. Inset right: parameter values used in the simulation. A scaling factor = 0.33 has been introduced. B−E: Simulations of $\bar{P}$, where the influence of the individual structural and spectroscopic parameters on $\bar{P}$ are investigated, by variation of one parameter at a time. The parameter values were the same as the fitted values of Figure 6, except for the parameter that was varied, for which still the mean of the parameter values for the cis and the trans form was kept the same as the fitted value of Figure 6. The κ^2 orientation factors for the acceptor being in a trans and a cis conformation, denoted by $\kappa^2(N,\Delta_{bp})$ and $\kappa^2(P,\Delta_{bp})$ (eq 21), have been assumed to be constant and equal $^2/_3$ and the factor α (eqs 16 and 22) has been set to one, if not stated otherwise. In all figures, a scale factor has been introduced (=0.33), and the experimental $\bar{P}$ (solid line, solid squares) and a simulated $\bar{P}$, where all parameters are identical for the cis and trans forms (solid line), have been introduced for reference. B: Effects of different normal separation distances d_{rA} for the trans and cis conformations. Dotted line: $d_{rA}(N) = 10$ Å, $d_{rA}(P) = 2$ Å. Dashed line: $d_{rA}(N) = 2$ Å, $d_{rA}(P) = 10$ Å C: Effects of different radial orientations Ψ for the trans and cis forms, where $(\Psi(N) + \Psi(P))/2 = 308°$. Dotted curves, with increasing amplitudes: $\Delta\Psi = \Psi(P) - \Psi(N) = 60°$, 120°, and 180°. Dashed curves, with increasing amplitudes: $\Delta\Psi = \Psi(P) - \Psi(N) = -60°$, −120°, and −180°. D: Isolated effects of the differences in L ($\Delta L = 9$ Å, with $L(N) = -0.5$ Å, $L(P) = 8.5$ Å, dotted line) and â ($\mathbf{a_1}(N) = 0.85$, $\mathbf{a_2}(N) = 0.15$, and $a_1(P) = 0.3$, $\mathbf{a_2}(P) = 0.7$, dashed line) used in the simulation of Figure 8A. E: Effects of the spectroscopic parameters $\alpha < 1$ (here set to 0.75, which was used in the simulation of Figure 8A (dotted line)) and $\delta > 1$ (dashed line).

the parameter values in the simulation consistent with those obtained in the fit of eq 28 (Figure 6), the parameter values from that fit were used for both conformations, except for the values of d_{rA}, Ψ, and L. For these parameters, the mean values for the two conformations were kept the same as the fitted parameter values in Figure 6. For Ψ, no improvement of the simulation could be found upon deviation from its fitted value (see Figure 8C). The parameter values used in the simulation are given in Figure 8A. Clearly, a simulation of this kind cannot provide precise information about the orientations of the dyes. Still, it shows that differences in the orientation and length of the linker arm, and in the κ^2 orientation factor for the trans and cis conformation of the acceptor dye can generate a periodic variation and an overall increase of $\bar{P}$, well compatible with the experimental findings.

In a next step, the influence of the individual structural and spectroscopic parameters on $\bar{P}$ were investigated by simulations, where the parameters were varied one by one (Figures 8B−E). For the parameter varied, the mean value for the cis and the trans form was kept the same as the fitted value from Figure 6. The values of the other structural parameters were the same for both the trans and the cis conformation, and identical to those of Figure 6. The κ^2 orientation factor was set to $^2/_3$ for both the trans and the cis forms, if not stated otherwise (Figure 8D).

4.7.3. Simulation of $\bar{P}$: Effects of Structural Parameters. Figure 8B shows the influence of differences between the trans

and cis forms in d_{rA}. If d_{rA} is longer for the cis than for the trans form, i.e., $\Delta d_{rA} > 0$, a periodicity of $\bar{P}$ with the same period and phase as that experimentally observed can be produced. In contrast, if $\Delta d_{rA} < 0$, a $\bar{P}$ is produced, which is totally out of phase with the observed $\bar{P}$. For a given difference in the length of d_{rA} between the cis and trans forms, the phase of $\bar{P}$ can be shifted by variation of the radial orientation Ψ of the normal separation vector for both forms (not shown).

In Figure 8C, simulations are shown with different Ψ for the trans and cis forms, but with the mean value of Ψ kept the same for the two forms. A periodic variation of $\bar{P}$ is then generated, with a period of 10bp, but out of phase with the experimental $\bar{P}$. The amplitudes of the periodic variation increases with larger separation in Ψ between the trans and cis isomers.

The experimentally found periodicity of $\bar{P}$ is thus well in agreement with a situation, where the trans form of the acceptor dye is closer to the DNA helical axis than the cis conformation ($\Delta d_{rA} > 0$), and where Ψ equals the fitted value from Figure 6 for both conformations, ($\Delta\Psi = 0$).

In Figure 8D two simulations are plotted, which show the individual effects of differences in the κ^2 orientation factor and in L between the two conformational forms of the acceptor dye. When L is shorter for the trans than for the cis form ($\Delta L > 0$), an overall increase of $\bar{P}$ is produced, similar to the increase observed experimentally. In contrast, when L is longer for the trans form ($\Delta L < 0$) an overall decrease of $\bar{P}$ is generated (simulation not shown).

The κ^2 orientation factor can be influenced both by the relative radial orientations of the transition moments of the donor and acceptor dyes, as well as by the axial distance between the dyes. In the first case, a periodic modulation is generated and in the second case an overall change of $\bar{P}$ can be expected as a function of Δ_{bp}. For those simulations of $\bar{P}$ best resembling the experimental data, the κ^2 orientation factor was calculated based on a predominant orientation of the transition dipole moment of the trans form parallel to, and that of the cis conformation predominantly oriented perpendicular to the DNA helical axis (Figures 7C and 8A). The κ^2 orientation factor was then mainly found to contribute to an overall increase of $\bar{P}$ (Figure 8D, dashed line). On the basis of our model, an overall nonperiodic change of κ^2 with increasing Δ_{bp} can be attributed to a change in the angle Θ_A between the transition moment of the acceptor $\hat{a}$ and the donor−acceptor separation vector $R_{DA}\hat{r}$ (eq 30). As can be seen from Figure 7C, the change in Θ_A is related to the magnitude of d_{rA} and d_{rD}. The change is small when the axial distance between the labeling sites, $R_z = L + \Delta_{bp}z_{bp}$, is much longer than d_{rA} and d_{rD}, while relatively large changes in Θ_A can be expected when d_{rA} and d_{rD} are longer or comparable to R_z.

4.7.4. Electrostatic Considerations on the Simulated Data. With both d_{rA} and L shorter for the trans than for the cis form, it is likely that the trans form of the acceptor dye to a larger extent folds back onto the linker arm than does the cis form. This is also supported by electrostatic considerations. In Figure 9A, the structures of the trans and cis form of the Cy5 dye molecule are shown. At each of the headgroups of the dye there is a negatively charged sulfonic acid group, as well as a nitrogen, that together with the nitrogen of the other headgroup harbor one positive charge. Altogether, the Cy5 molecule is negatively charged. The charge distribution within the molecule depends on its conformation. While significant in the trans form, the net electric dipole moment in the cis state is very small. Via a linker arm, the Cy5 molecule is coupled to the negatively charged phosphate group of the 5′-end of the DNA strand (Figure 9B). In a trans form, the nitrogen of the distal headgroup is facing toward the linker arm, and the sulfonic acid group is turned away from it. The resulting electrostatic attraction, together with the interaction of a net electric dipole moment of the dye molecule, then promotes a folding of the dye toward the linker arm (Figure 9B). On the other hand, in a cis conformation, the distal headgroup is turned 180°, and the sulfonic group is instead facing toward the linker arm. This, in combination with a negligible net electric dipole moment, would rather lead to a repulsion of the distal headgroup from the linker arm, so that both d_{rA} and L are longer for the cis than for the trans conformation (Figure 9B).

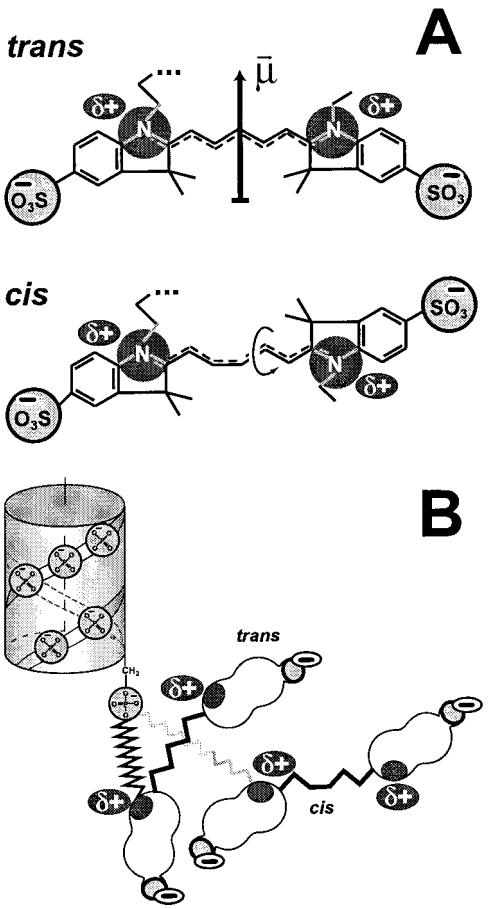

Figure 9. Possible interactions between the acceptor dye, the linker arm and the DNA molecule. A: Charge distributions for Cy5 in a trans and in a cis conformation. μ denotes the net electric dipole moment present in the trans form. B: Possible spatial arrangement of the Cy5 molecule in a trans and in a cis conformation with respect to the linker arm and DNA molecule. See text for further details.

4.7.5. Relation of Simulated κ^2 to Acceptor Fluorescence Anisotropy Data. In general, FRET-mediated excitation strongly reduces the fluorescence anisotropy compared to direct excitation. One reason is that, after excitation of the donor, the fluorescence emission is preceded by rotational diffusion of both dyes. In addition, when $R_{DA} \ll R_0$, the FRET efficiency will be close to unity, and relatively independent of the orientation of the acceptor dye, which generates a close to isotropic acceptor fluorescence. In Figure 8A, the measured steady-state anisotropy of the acceptor dye fluorescence r_A as a function of Δ_{bp} is plotted. The r_A plotted is corrected for direct excitation of the acceptor and cross-talk of donor fluorescence. As expected, r_A is close to zero for $\Delta_{bp} < 13$bp, which indicates that the acceptor dye can be excited via FRET relatively independent of its

orientation. For $\Delta_{bp} = 13-17$bp, where R_{DA} approximates R_0, a distinct increase in r_A can be noted, indicating that the extent of FRET start to depend on the orientation of the dyes. In this range, the slope of E vs Δ_{bp} is relatively steep (see Figure 6), which should select for the most favorable orientations of â within the range of orientations possible for a given Δ_{bp}, and thereby lead to an increased r_A. For $\Delta_{bp} > 17$ bp, a slight decrease in r_A can be noticed. This can be attributed to a periodic modulation of the κ^2 orientation factor, following from the change of the radial orientation of â with Δ_{bp}. Alternatively, for large Δ_{bp}, the relative changes of E are smaller, and so are the relative changes of Θ_A, which reduces the dependence of the κ^2 orientation factor on the axial distance (see section 4.7.1 and Figure 7C). Then a larger range of orientations for a certain Δ_{bp} will show similar FRET-efficiencies, which should also lead to the observed reduction in r_A. Since only the trans conformation of the acceptor dye should be fluorescent, the anisotropy of the acceptor fluorescence reflects the anisotropy of the acceptor dyes being in a trans conformation.

The measured r_A of Figure 8A supports the steady-state anisotropy data measured under direct excitation (Table 2) that the orientation of the acceptor dye is not isotropic, at least not in the trans form. Moreover, it is compatible with a predominant orientation of the trans acceptor dye along the helical axis, and provides evidence that variations and differences in κ^2 between the trans and cis form are mainly present for long R_{DA}. The measured r_A indicates that the extent to which FRET occurs depends very weakly on the orientation of the dyes until Δ_{bp} reaches the range of 13−17 bp. Orientational differences between the trans and cis conformation of the acceptor should also not be evident as a change of $\bar{P}$ for lower Δ_{bp}. This agrees well with the measured $\bar{P}$ (Figure 8A), for which an overall increase is observed, which coincides with that of r_A.

4.7.6. Simulation of $\bar{P}$: Effects of Absorption Spectrum Changes Following Isomerization. At this point, it can be concluded that structural and orientational factors can generate the experimentally observed variations of $\bar{P}$ over Δ_{bp}. However, they cannot explain why the amplitudes of $\bar{P}$ under FRET-mediated excitation were found to be generally much lower than those measured under direct excitation of the acceptor dyes. In particular, when $R_{DA} \ll R_0$, $E(N)$ and $E(P)$ can be expected to be close to unity, and only very small changes of $\bar{P}$ can be generated from structural effects, no matter what orientations and positions the two conformations of the acceptor dye have with respect to each other. To take this general reduction of $\bar{P}$ into account, a scaling factor for $\bar{P}$ had to be introduced in the simulations (0.33 for the simulations shown). This motivates a discussion what the underlying mechanisms of this scaling factor can be.

A blue-shift of the excitation spectrum of the cis-isomer relative to that of the trans form ($\delta > 1$, see eqs 21) would lead to a stronger spectral overlap with the donor emission spectrum for the cis than for the trans isomer. This would favor $E(P)$ relative to $E(N)$, and thus k'_{BISO} relative to k'_{ISO} (eqs 13 and 14), and a lower amplitude of $\bar{P}$ can be expected (eq 20). However, $\delta > 1$ only leads to a reduction of $\bar{P}$ for $R_{DA} \approx R_0$ or longer, and not to a general reduction of $\bar{P}$ (Figure 8E). Moreover, the reduction in $\bar{P}$ under FRET-mediated excitation is far more prominent than that seen under direct excitation at 496 nm. Therefore, the influence of a shift in δ is small and cannot account for a major reduction in $\bar{P}$.

The factor α, defined as the ratio of the excitation cross section of the cis over that of the trans form, σ_P/σ_N (eq 16), can also have an influence on the measured $\bar{P}$. However, the simulation in Figure 8E shows that if $\alpha < 1$, $\bar{P}$ would be reduced only for short R_{DA}, while for $R_{DA} > R_0$ practically no effect on $\bar{P}$ is seen. In addition, also for short R_{DA} an $\alpha < 0.5$ would be needed to generate a relative shift in $\bar{P}$ comparable to that observed. Such a low value of α would not be in line with what has previously been reported for cyanine dyes similar to Cy5, where an α close to unity was found.[44−46]

4.7.7. Simulation of $\bar{P}$: Additional Effects. The general reduction of $\bar{P}$ is not due to structural parameters, and can also not be fully generated from spectroscopic effects, such as a shift of α or δ. Therefore, additional, in particular photochemical, effects have to be considered. An additional photochemically induced deactivation of the cis conformation, present under FRET-mediated excitation, but not under direct excitation of the acceptor dyes, would not only explain a general reduction of $\bar{P}$, but would also give a reason for the overestimation of the FRET efficiencies found after normalization of the isomerization rates according to eq 19. One possible mechanism for such a cis state deactivation is charge transfer in the DNA molecule, which have been observed to take place over distances as long as 200 Å. Although the details of the mechanisms are still under debate, the rate of transfer has been found to be relatively insensitive to Δ_{bp}.[54−56] Under FRET-mediated excitation, it would therefore be possible that free charges are generated from excitation of the donor dyes, and that they propagate along the DNA chain. From the redox potentials,[57] it is known that Cy5 can be oxidized by nucleobase radical ions, and in the case of stilbenes, isomerization of radical cations is known to take place, with yields that can be significantly different from those seen in the absence of radical formation.[58] It is therefore possible that Cy5 radical cations can be formed and, prior to charge recombination, that they undergo isomerization and back-isomerization. If the radical cation of Cy5 would have a yield of back-isomerization which is favored over that of isomerization, an increased population of trans isomers and a reduction of $\bar{P}$ would follow. However, clearly further investigations are needed to reveal the identity and the details of the mechanism behind this general reduction of $\bar{P}$.

5. Conclusions and Outlook

In this study, we have introduced and investigated two concepts for how FCS can be used to characterize FRET. In the first approach, FRET efficiencies were determined from the detected acceptor fluorescence rate per molecule under study. As a second possibility, the fluorescence fluctuations of the detected acceptor fluorescence generated from trans−cis isomerization kinetics were utilized.

The concept to determine the FRET efficiency from the relative increase in acceptor fluorescence is well established. The advantage of FCS is that the absolute mean number of molecules within the detection volume can be determined making a concentration calibration superfluous. However, the use of this approach is limited to samples where one can control the influence from other light sources than FRET-induced acceptor fluorescence and requires careful calibrations of cross-talk and background. Also, labeling efficiencies of the donor and acceptor fluorophores have to be considered. An absolute determination of FRET efficiencies is difficult to perform, since the total detection quantum yield of the instrumentation g is difficult to determine with high enough precision and accuracy. Nonetheless, for the measurements presented in this study, where the background and the donor emission cross-talk were almost negligible, the relative FRET-efficiencies determined with this approach were found to scale well with those determined via the isomerization kinetics of the acceptor dye.

To our knowledge, the concept to measure FRET efficiencies via the trans−cis isomerization kinetics is completely new. In principle, characterizing FRET by FCS and via the isomerization kinetics offers several advantages. The measured k_{ISOtot} is independent of labeling efficiencies of both the donor and the acceptor, of donor fluorescence leaking into the detection channels for the acceptor fluorescence, of background, as well as of the absolute concentration of the measured molecules. Thus, no prior purification of double labeled molecules is needed, in contrast to conventional steady-state ensemble measurements, where great care must be taken to purify the molecules containing both donor and acceptor dyes. Even if the donor fluorescence, or a high background, would dominate over the signal in the detectors for the acceptor fluorescence, they would not generate the specific fluorescence fluctuations seen for the acceptor fluorescence. The relaxation rate of the isomerization process k_{ISOtot} only depends on the excitation rate of the acceptor dye. For FRET measurements in general, the number of measurements on separate solutions with different molecules should be kept to a minimum, to avoid generating unnecessary measurement noise, system errors etc.[5] Still, FRET measurements based on changes in donor and acceptor fluorescence quantum yields typically requires rather elaborate spectral component analyses of donor-only, acceptor-only, as well as of donor−acceptor-labeled molecules.[7] With the approach presented here, control measurements can be kept to a minimum due to the relative independence of k_{ISOtot}. Moreover, in contrast to single molecule or ensemble FRET measurements based on changes in the donor and/or acceptor fluorescence, no knowledge about the absolute detection quantum yield of the instrumentation is required. The instrumentation needed for our approach can be made quite robust and simple, and since it is a confocal microscopy-based technique it can be applied to a wide range of different environments. For determination of the FRET efficiencies via the quenching of the donor fluorescence lifetime, it is usually necessary to determine the fluorescence lifetimes for both the donor−acceptor as well as for the donor-only labeled molecules, since fluorescence lifetimes can be extremely environment-dependent. The environmental sensitivity of the isomerization process must also be considered in FRET measurements by FCS, but the calibration can also be done by direct excitation on the same sample.

However, in practice, absolute calibration is not so easy to perform with high accuracy. In this study, the calibration of the isomerization rates measured under FRET-mediated excitation with those measured under direct excitation lead to a significant overestimation of the absolute FRET-efficiencies. The reason for this is not fully clear. Systematic errors in the determination of the excitation intensity experienced by the molecules under study can contribute. However, we estimate the relative error of the measured excitation intensities to less than 20%. Therefore, it is more likely that the overestimation is due to additional photochemical pathways not taken into consideration in the derivation of the FRET efficiencies from the experimental parameters. The fact that the FRET-efficiencies are overestimated, in combination with the finding that the amplitude of $\bar{P}$ is much lower under FRET-mediated excitation suggests that an additional photochemical deactivation pathway of the cis state may be involved. Here, charge transfer from the excited donor to the acceptor dye, via the DNA chain could be a possible mechanism. However, further investigations are needed to verify this theory.

Although it is difficult to accurately determine the absolute FRET efficiencies of the molecules under study, the presented data show that relative FRET efficiencies can be measured over a broad range of donor−acceptor distances (4−22 bp corresponding to approximately 13−75 Å with 3.4 Å/bp), with a precision good enough that two samples with oligonucleotides differing in the donor−acceptor distances by only 1−2bp can be well separated over the whole range of distances. The lower limit for what FRET efficiencies that can be measured is set by thermal deactivation of the cis isomer to the trans form. At low FRET efficiencies, where the excitation induced transitions between the trans and cis isomers are also low, a possible influence of thermal deactivation of the cis state should be kept in mind. However, no significant contribution of such a process could be noticed, not even for longer donor−acceptor distances measured at excitation intensities down to 0.6 kW/cm^2.

For the measured $\bar{P}$, a periodic variation and an overall increase in $\bar{P}$ with longer Δ_{bp} could be observed. We show by simulations that differences in the position and orientation of the trans and cis form of the acceptor dye can underlie the periodicity as well as the overall increase of $\bar{P}$, and thereby provide additional structural information.

Although the population of cis-isomers was found to be lower under FRET-mediated excitation than under direct excitation of the acceptor dyes, the loss of acceptor fluorescence due to population of nonfluorescent, but still FRET-active, cis states is significant. This should be kept in mind when cyanine dyes are used as acceptor dyes, in particular when the acceptor fluorescence is used as a read-out parameter. In this study, the differences in FRET efficiencies between the isomeric forms are not likely to be very big, as seen from the plots of the relative FRET efficiencies measured via isomerization kinetics (reflecting a weighted sum of E(N) and E(P)) compared to those from fluorescence rates per molecule (reflecting E(N)). However, depending on their relative orientations and positions, bigger differences in E between the isomeric forms are in principle possible. The measured FRET efficiency, would then depend on if E(N) or a weighted sum of E(N) and E(P) are reflected in the read-out parameter. (For instance, when the FRET efficiency is determined via the acceptor fluorescence, E(N) is measured, since only the trans form is fluorescent. If on the other hand the FRET efficiency is determined via donor fluorescence lifetime quenching, a contribution from the FRET-active acceptor dyes in a cis conformation should also be expected.) It is interesting to note that almost no attention has previously been paid in the literature to these considerations.[37]

Finally, it should be pointed out that FCS is well suited to monitor several photodynamic features and photoinduced transient states, involving both the donor and the acceptor dyes. Since several of these states can be influenced by FRET, FCS can in principle also be used to monitor the presence and extent of FRET via these states. For the donor dye, the quantum yield of a process originating from the excited state will decrease in the presence of FRET, since FRET is a competing deactivation process of the excited state of the donor. For instance, we could note that at higher excitation intensities the triplet state build-up in the donor molecules, measured via AC curves of the donor fluorescence, was lower in oligonucleotides with short Δ_{bp} and high FRET efficiencies, compared to oligonucleotides with a low E or no FRET at all. In contrast, for the acceptor dye a process originating from the excited state will be promoted by FRET, since FRET does not compete in the deactivation of the excited state, and since excitation is a prerequisite for the generation of the state at all. Monitoring fluctuations on the acceptor side has the advantage that incomplete labeling is automatically corrected, since basically only those acceptor dyes are seen which have been excited via FRET (if direct excitation of the acceptor dyes is negligible). An important advantage using trans−cis fluctuations to monitor FRET is that the relative population of the cis state remains more or less constant over

the whole range of excitation rates. The relaxation process is therefore clearly visible also for low FRET efficiencies, where it for instance would be difficult to detect a triplet state population, and even more difficult to derive any information about the extent of FRET from its amplitude and relaxation time. Finally, it should be mentioned that cyanine dyes are not the only dyes having transient states with photodynamic features like those of isomerization. Recently, it has been shown by FCS measurements that green fluorescent proteins have similar photodynamic properties.[35,36] The approach presented here is therefore not restricted only to the group of cyanine dyes as acceptor fluorophores.

Appendix 1

For a Cartesian coordinate system ($\hat{x}$, $\hat{y}$, $\hat{z}$), where $\hat{z}$ is along the DNA helical axis, $\hat{x}$ is along the direction of the normal separation vector from the helical axis to the acceptor dye, and $\hat{y}$ is perpendicular to $\hat{x}$ and $\hat{z}$:

$$\hat{a}_{para} = (0, 0, 1) \tag{A1}$$

$$\hat{a}_{perp} = (1, 0, 0) \tag{A2}$$

$$\hat{r} = (r_x, r_y, r_z) = \frac{1}{R_{DA}}(d_{rA} - d_{rD}\cos\Theta, d_{rD}\sin\Theta, L + \Delta_{bp}z_{bp}) \tag{A3}$$

where R_{DA} is given by eq 27 and $\Theta = \Psi + \Delta_{bp}\phi_{bp}$. Given that the emission dipole moment of the donor is isotropic, and the excitation dipole moment of the acceptor is fixed in a linear direction, the κ^2 orientation factor can be expressed as[4] (eq 30):

$$\kappa^2 = {}^1/_3 + (\hat{a} \cdot \hat{r})^2$$

Then, for $\hat{a} = \hat{a}_{para}$,

$$\kappa^2(para) = {}^1/_3 + (\hat{a}_{para} \cdot \hat{r})^2 = {}^1/_3 + r_z^2 \tag{A4}$$

and for $\hat{a} = \hat{a}_{perp}$,

$$\kappa^2(perp) = {}^1/_3 + (\hat{a}_{perp} \cdot \hat{r})^2 = {}^1/_3 + r_x^2 \tag{A5}$$

The κ^2 orientation factors with the acceptor in a trans or in a cis form we form as

$$\kappa^2(X) = \mathbf{a_1}\kappa^2(perp) + \mathbf{a_2}\kappa^2(para) \tag{A6}$$

where X is either N or P and $\mathbf{a_1}$ and $\mathbf{a_2}$ can be different for the two forms. To calculate $\bar{P}$, the κ^2 orientation factors of eq A6 are included in $\beta_N(\Delta_{bp})$ and $\beta_P(\Delta_{bp})$ of eq 21, which are put into the expression for $\bar{P}(\Delta_{bp})$ of eq 22, in which the expression for R_{DA} is given by eq 27.

References and Notes

(1) Perrin, J. *Ann. Phys. (Paris)* **1932**, *17*, 283.
(2) Förster, T. *Ann. Phys.* **1948**, *2*, 55.
(3) Stryer, L.; Haugland, R. P. *Proc. Natl. Acad. Sci. U. S. A.* **1967**, *58*, 719.
(4) Van Der Meer, B. W.; Coker, G., III; Chen. S. Y. S. *Resonance Energy Transfer*; VCH Publishers: New York. 1994.
(5) Clegg. R. M. *Methods in Enzymology*; Academic Press: New York, 1992.
(6) Wu, P.; Brand, L. *Anal. Biochem.* **1994**, *218*, 1.
(7) Selvin. P.; *Methods in Enzymology*; Academic Press: New York, 1995.
(8) Szöllösi, J.; Damjanovich, S.; Matyus, L. *Cytometry* **1998**, *34*, 159.
(9) Keller, R. A.; Ambrose, P.; Goodwin, P. M.; Jett, J. H.; Martin, J. C.; Wu, M. *Appl. Spectrosc.* **1996**, *50*, 12A.
(10) Ambrose, W. P.; Goodwin, P. M.; Jett, J. H.; Van Orden, A.; Werner, J. H.; Keller, R. A. *Chem. Rev.* **1999**, *99*, 2929.
(11) Weiss, S. *Science* **1999**, *283*, 1676.
(12) Ha, T.; Enderle, T.; Ogletree, D. F.; Chemla, D. S.; Selvin, P. R.; Weiss, S. *Proc. Natl. Acad. Sci. U. S. A.* **1996**, *93*, 6264.
(13) Ha, T.; Ting, A. Y.; Liang, J.; Caldwell, W. B.; Deniz, A. A.; Chemla, D. S. *Proc. Natl. Acad. Sci. U. S. A.* **1999**, *96*, 893.
(14) Deniz, A. A.; Dahan, M.; Grunwell, J. R.; Ha, T.; Faulhaber, A. E.; Chemla, D. S.; Weiss, S.; Schultz, P. G. *Proc. Natl. Acad. Sci. U. S. A.* **1999**, *96*, 3670.
(15) Ha, T.; Zhuang, X.; Kim, H. D.; Orr, J. W.; Williamson, J. R.; Chu, S. *Proc. Natl. Acad. Sci. U. S. A.* **1999**, *96*, 9077.
(16) Dahan, M.; Deniz, A. A.; Ha, T.; Chemla, D. S.; Schultz, P. G.; Weiss, S. *Chem. Phys.* **1999**, *247*, 85.
(17) Ha, T.; Ting, A. Y.; Liang, J.; Deniz, A. A.; Chemla, D. S.; Schultz, P. G.; Weiss, S. *Chem. Phys.* **1999**, *247*, 107.
(18) Jia, Y.; Talaga, D. S.; Lau, W. L.; Lu, H. S. M.; DeGrado, W. F.; Hochstrasser, R. M. *Chem. Phys.* **1999**, *247*, 69.
(19) Ishii, Y.; Yoshida, T.; Funatsu, T.; Wazawa, T.; Yanagida, T. *Chem. Phys.* **1999**, *247*, 163.
(20) Magde, D.; Elson, E. L.; Webb, W. W. *Phys. Rev. Lett.* **1972**, *29*, 705.
(21) Elson, E. L.; Magde, D. *Biopolymers* **1974**, *13*, 1.
(22) Magde, D.; Elson, E. L.; Webb, W. W. *Biopolymers* **1974**, *13*, 29.
(23) Ehrenberg, M.; Rigler, R. *Chem. Phys.* **1974**, *4*, 390.
(24) Rigler. R.; Widengren. J. *Bioscience*; Klinge, B., Owman, C., Eds.; Lund University Press: Lund, 1990.
(25) Rigler. R.; Widengren. J.; Mets. Ü. *Fluorescence Spectroscopy*; Wolfbeis O. S., Ed.; Springer-Verlag: Berlin, 1992.
(26) Rigler, R.; Mets, Ü.; Widengren, J.; Kask, P. *Eur. Biophys. J.* **1993**, *22*, 169.
(27) Thompson. N. L. *Topics in Fluorescence Spectroscopy*; Lakowicz, J. R., Ed.; Plenum Press: New York, 1995.
(28) Maiti, S.; Haupts, U.; Webb, W. W. *Proc. Nat. Acad. Sci. U. S. A.* **1997**, *94*, 11753.
(29) Widengren, J.; Rigler, R. *Cell. Mol. Biol.* **1998**, *44*, 857.
(30) Van Craenenbroeck, E.; Engelborghs, Y. *J. Mol. Recogn.* **2000**, *13*, 93.
(31) Mets, Ü.; Widengren, J.; Rigler, R. *Chem. Phys.* **1997**, *218*, 191.
(32) Widengren, J.; Dapprich, J.; Rigler, R. *Chem. Phys.* **1997**, *216*, 417.
(33) Widengren, J.; Rigler, R.; Mets, Ü. *J. Fluoresc.* **1994**, *4*, 255.
(34) Widengren, J.; Mets, Ü.; Rigler, R. *J. Phys. Chem.* **1995**, *99*, 13368.
(35) Widengren, J.; Mets, Ü.; Rigler, R. *Chem. Phys.* **1999**, *250*, 171.
(36) Schwille, P.; Kummer, S.; Heikal, A. A.; Webb, W. W. *Proc. Natl. Acad. Sci. U. S. A.* **2000**, *97*, 151.
(37) Widengren, J.; Schwille, P. *J. Phys. Chem. A* **2000**, *104*, 6416.
(38) Widengren, J.; Rigler, R. *Bioimaging* **1996**, *4*, 149.
(39) Eggeling, C.; Widengren, J.; Rigler, R.; Seidel, C. *Anal. Chem.* **1998**, *70*, 2651.
(40) Haas, E.; Steinberg, I. Z. *Biophys. J.* **1984**, *46*, 429.
(41) Brasselet, S.; Peterman, E. J. G.; Miyawaki, A.; Moerner, W. E. *J. Phys. Chem. A* **2000**, *104*, 3676.
(42) Eggeling, C.; Fries, J.; Brand, L.; Guenther, R.; Seidel, C. A. M. *Proc. Natl. Acad. Sci. U. S. A.* **1998**, *95*, 1556.
(43) Arago'n, S. R.; Pecora, R. *J. Chem. Phys.* **1976**, *64*, 1791.
(44) Dempster, D. N.; Morrow, T.; Rankin, R.; Thompson, G. F. *J. Chem. Soc., Faraday Trans.* **1971**, *68*, 1479.
(45) Vaveliuk, P.; Scaffardi, L. B.; Duchowicz, R. *J. Phys. Chem.* **1996**, *100*, 11630.
(46) Bilmes, G. M.; Tocho, J. O.; Braslavsky, S. E. *J. Phys. Chem.* **1988**, *92*, 5958.
(47) Amersham Pharmacia, product information, 2000.
(48) Sauer, M.; Angerer, B.; Han, K. T.; Zander, C. *Phys. Chem. Chem. Phys.* **1999**, *1*, 2471.
(49) Korobov, V. E.; Chibisov, A. K. *Russ. Chem. Rev.* **1983**, *52*, 27.
(50) Haughland. R. *Handbook of Fluorescent Probes and Research Chemicals*; Molecular Probes, Inc.: Eugene, Oregon, 2000.
(51) Schweinberger, E.; Widengren, J.; Berger, S.; Eggeling, C.; Schaffer, J.; Seidel, C. A. M. Submitted for publication.
(52) Clegg, R. M.; Murchie, A. I. H.; Zechel, A.; Lilley, D. M. *Proc. Natl. Acad. Sci. U. S. A.* **1993**, *90*, 2994.
(53) Jares-Erijman, E. A.; Jovin, T. M. *J. Mol. Biol.* **1996**, *257*, 597.
(54) Berlin, Y. A.; Burin, A. L.; Ratner, M. A. *J. Phys. Chem. A* **2000**, *104*, 443.
(55) Jortner, J.; Bixon, M.; Langenbacher, T.; Michel-Beyerle, M. E. *Proc. Natl. Acad. Sci. U. S. A.* **1998**, *95*, 12759.
(56) Grinstaff, M. W. *Angew. Chem. Int. Ed.* **1999**, *38*, 3629.
(57) Seidel, C. A. M.; Schulz, A.; Sauer, M. H. M. *J. Phys. Chem.* **1996**, *100*, 5541.
(58) Waga, M.; Maki, S.; Hashimoto, F.; Sakuragi, H. *Chem. Phys. Lett.* **1997**, *265*, 277.